NEUROSCIENCE

Subthreshold repetitive transcranial magnetic stimulation induces cortical layer–, brain region–, and protocol-dependent neural plasticity

Rebecca C. S. Ong[1,2] and Alexander D. Tang[1,2,3]*

Repetitive transcranial magnetic stimulation (rTMS) is commonly used to study the brain or as a treatment for neurological disorders, but the neural circuits and molecular mechanisms it affects remain unclear. To determine the molecular mechanisms of rTMS and the brain regions they occur in, we used spatial transcriptomics to map changes to gene expression across the mouse brain in response to two commonly used rTMS protocols. Our results revealed that rTMS alters the expression of genes related to several cellular processes and neural plasticity mechanisms across the brain, which was both brain region– and rTMS protocol–dependent. In the cortex, the effect of rTMS was dependent not only on the cortical region but also on each cortical layer. These findings uncover the diverse molecular mechanisms induced by rTMS, which will be useful in interpreting its effects on cortical and subcortical circuits.

INTRODUCTION

Repetitive transcranial magnetic stimulation (rTMS) is an extremely attractive tool in both basic and clinical neuroscience as there are very few tools that can noninvasively alter neural activity and neural plasticity in the human brain. However, despite its long-standing use and widespread popularity, it remains unclear how rTMS affects neural circuits across the brain and why rTMS outcomes can vary with different rTMS protocols (e.g., stimulation pattern). As a result, interpreting the effect of rTMS on neural processes and selecting which rTMS protocols to treat specific pathologies is challenging. Therefore, characterizing the effect of rTMS across the brain following different stimulation protocols is needed to make more informed interpretations of rTMS neuromodulation and provide an evidence base to select which rTMS protocol should be used to produce specific effects.

Using rodent models, it is known that rTMS induces both neuronal and glial plasticity mechanisms. For example, in entorhinohippocampal slice cultures, 10-Hz magnetic stimulation induces functional synaptic plasticity (*1*–*3*) that requires the release of microglial factors (*4*). In vivo, rTMS in the form of intermittent theta burst stimulation (iTBS) to the adult mouse sensorimotor cortex induces structural synaptic plasticity (altered dendritic spine density and rate of formation and removal) in layer 2/3 and 5 pyramidal neurons (*5*) as well as oligodendrocyte plasticity in several cortical regions and the corpus callosum (*6*, *7*). However, it remains unclear how these plasticity mechanisms vary with the rTMS protocol used, if multiple neural plasticity mechanisms are induced simultaneously, and if regions outside the stimulated region also undergo the same plastic changes. Furthermore, given the heterogeneity in the structural and cellular composition of different brain regions and cortical layers, it is likely that the effect of rTMS is not uniform across the brain. This is at least true of oligodendrocyte plasticity as iTBS has been shown to increase the number of new oligodendrocytes in the cortex but only in very superficial and deep cortical layers (L1, L5, and L6) (*6*). With the intensity of the rTMS electric field decreasing in depth exponentially from the cortical surface (*8*), the cortical layer–specific changes cannot simply be explained by rTMS intensity differences and suggest that the cellular and structural features of a brain region can influence the rTMS plasticity induced. However, cortical layer–specific changes for other rTMS-induced plasticity mechanisms have not been investigated.

Electrophysiological and microscopy studies in rodents have substantially improved our understanding of the cellular mechanisms underlying rTMS neuromodulation, but these techniques are often limited to characterizing changes to one neural plasticity mechanism at a time in a specific cell type or brain region. Spatial transcriptomics (*9*), on the other hand, provides a powerful alternative to investigating the molecular mechanisms of rTMS as it can characterize changes to multiple neural plasticity mechanisms across several cortical and subcortical regions of the mouse brain at high resolution. In addition to resolving differences between brain regions, the high spatial resolution of spatial transcriptomics makes it possible to characterize rTMS neuromodulation of the cortex down to individual cortical layers. In this study, we leveraged the power of spatial transcriptomics to map the changes to cellular processes and neural plasticity induced across the adult mouse brain following rTMS to the primary motor cortex (M1) and somatosensory cortex (SS). In addition, we aimed to characterize whether rTMS induces different changes to the M1 and SS and how consistent these changes are across the cortical layers. Our study focuses on the theta burst stimulation (TBS) protocols as they are commonly used in both basic and clinical rTMS studies. We first show that rTMS neuromodulation of the cortex was not uniform as characterization of the gross changes to gene expression in the M1 and SS from all cortical layers with bulk RNA sequencing (RNA-seq) showed little to no changes in gene expression following continuous theta burst stimulation (cTBS) and iTBS, respectively, relative to sham stimulation. In contrast, the high resolution of spatial transcriptomics revealed that both cTBS and iTBS lead to significant changes in gene expression related to multiple cellular processes and neural plasticity mechanisms in the cortex, white matter tracts, and subcortex, with the exact changes dependent on the stimulation protocol, brain region, and cortical

[1]Experimental and Regenerative Neurosciences, The University of Western Australia, Perth, Australia. [2]Perron Institute for Neurological and Translational Sciences, Perth, Australia. [3]Pharmacology and Toxicology Discipline, School of Biomedical Sciences, The University of Western Australia, Perth, Australia.
*Corresponding author. Email: adtang.research@gmail.com

layer. In general, the effects of cTBS were mostly on general cellular and neuronal processes, whereas iTBS had a greater effect on oligodendrocyte plasticity–related genes.

RESULTS

Bulk RNA-seq of the cortex shows little to no effect of rTMS

To determine whether the effect of rTMS is largely uniform between neighboring cortical regions, we applied whole transcriptome bulk RNA-seq to dissected sensorimotor cortical tissue (i.e., M1 + SS dissected together) 3 hours after stimulation (Fig. 1, A and B). Previous microarray and immunohistochemistry rTMS data have reported changes in gene and protein expression in cultured neuronal cells as early as 2 to 5 hours following stimulation (*10*–*14*). Hence, we selected this time point of 3 hours to further investigate whether similar gene expression changes can be detected following stimulation delivered to freely moving animals. A principal components analysis (PCA) plot of the sequenced data displayed no distinct clustering of biological replicates in each stimulation group (Fig. 1C). In particular, our sham (i.e., control) samples exhibited a large degree of spread

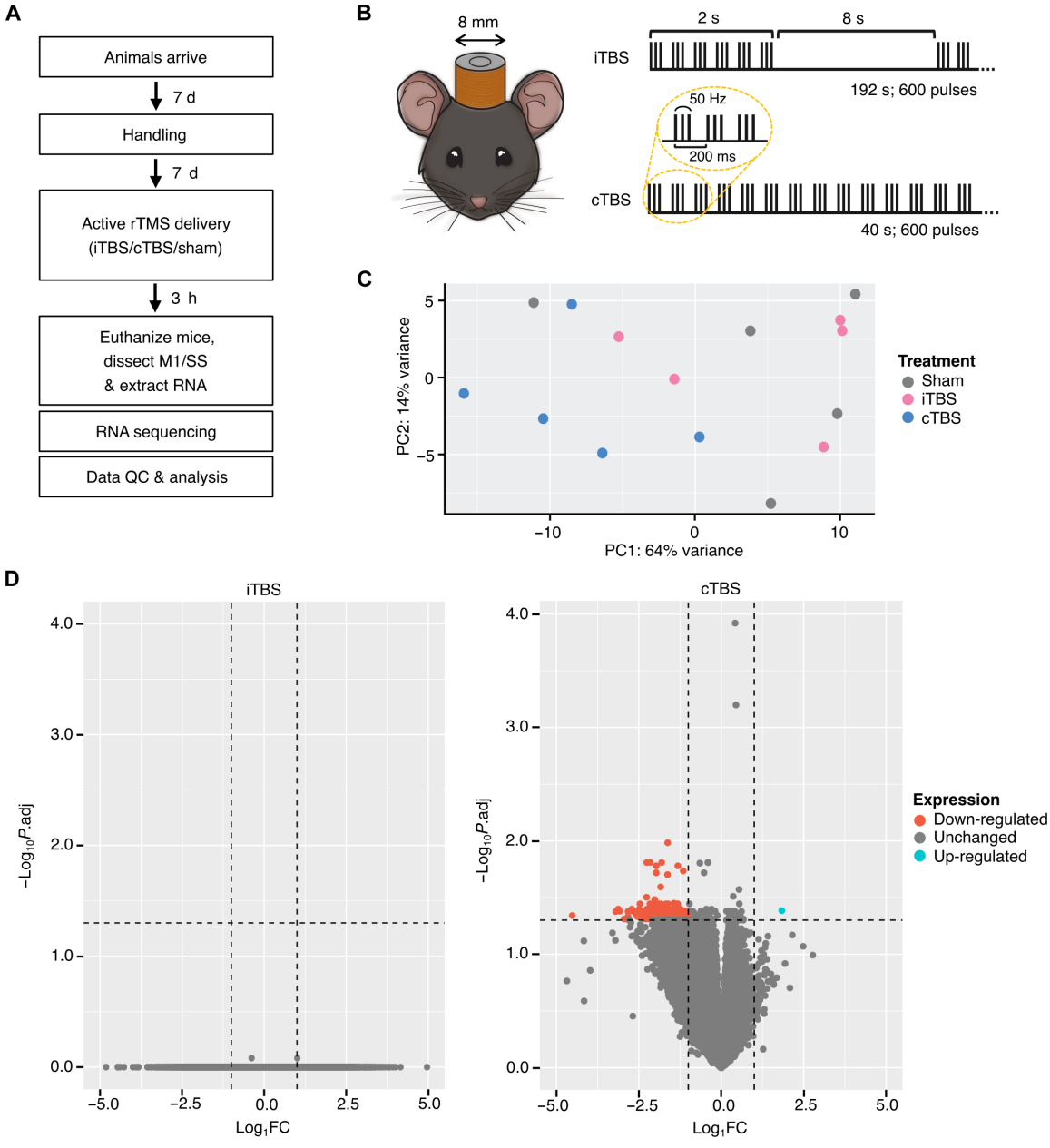

Fig. 1. Bulk RNA-seq indicates differences in the regulation of gene expression between iTBS and cTBS in the mouse cortex. (**A**) Experimental workflow for bulk RNA-seq of mice treated with iTBS ($n = 5$), cTBS ($n = 5$), or sham stimulation ($n = 5$). d, days; h, hours. (**B**) Schematic of the rTMS mouse model and stimulation protocols used. (**C**) Two-dimensional PCA plot reveals no distinct clustering between stimulation groups. (**D**) Volcano plots of DEGs show no effect of iTBS on gene expression in the cortex, whereas cTBS largely down-regulated the expression of cortical genes. After identifying DEGs, the Wald test was used to generate *P* values that were adjusted for multiple comparisons through the Benjamini-Hochberg false discovery rate correction.

on the PCA plot, reflecting an innate heterogeneity in our cohort of mice. Notwithstanding the variability within treatment groups, we found that cTBS accounted for the largest amount of variance between the conditions, with samples within this group clustering more distinctly on the PCA plot, away from iTBS and sham-stimulated animals. Therefore, this suggests that iTBS had a smaller effect on cortical gene expression profiles compared to cTBS. Reflecting this, differential expression analysis [*P*.adj ≤ 0.05 and absolute $\log_2$ fold change ($\log_2$FC) > 1] relative to sham stimulation revealed no changes in gene expression 3 hours following a single session of iTBS (Fig. 1D). In contrast, cTBS changed the expression of 293 genes with a $\log_2$FC threshold of > 1 (Fig. 1D). However, following the exclusion of predicted genes and pseudogenes, only 12 well-annotated protein-coding genes were identified to be differentially expressed following cTBS (1 up-regulated and 11 down-regulated) (Table 1).

To contextualize the functional implications of genes altered following cTBS, the differentially expressed genes (DEGs) were cross-referenced using the National Center for Biotechnology Information gene database to identify their function in the central nervous system (CNS). Genes involved in the regulation of synaptic transmission (*Atp6v1b1* and *Cacna1f*), DNA repair (*Rsf1os1*), and G protein–coupled receptor signaling (*Vmn2r84* and *Vmn2r86*) all had a reduced expression post-cTBS. *Crapb1* was the only significantly up-regulated gene, previously shown to be involved in several signaling pathways including the mitogen-activated protein kinase (MAPK) and calcium- and calmodulin-dependent protein kinase II (CamKII) pathways. Several genes had no identifiable function in the nervous system and were therefore left uncategorized. Because of the limited number of significant DEGs identified following cTBS, Gene Ontology (GO) enrichment analysis did not produce any common functional classes between genes.

Spatially profiling the transcriptional effects of TBS protocols

Given that bulk RNA-seq results indicated that iTBS and cTBS have no to some gross effect, respectively, on the transcriptional profile of the sensorimotor cortex 3 hours after stimulation, we hypothesized that rTMS could be inducing transcriptional changes at a finer resolution. Specifically, we hypothesized that rTMS induces changes that are spatially and substructure-specific (e.g., differences between motor and sensory cortices and differences between cortical layers) (*15*, *16*). Therefore, to further dissect the transcriptional changes with higher resolution and characterize changes to cortical and subcortical structures, we performed Visium spatial transcriptomics on coronal brain sections from iTBS, cTBS, and sham-stimulated mice (Fig. 2A).

Following batch correction, unsupervised clustering analysis was performed, which revealed 16 unique clusters across all iTBS, cTBS, and sham samples (Fig. 2, B and C). These clusters were manually annotated based on their anatomical location, using the Allen Mouse Brain Atlas as a reference (Fig. 2B), resulting in the allocation of clusters to various cortical layers [layer 1 (Ctx L1), layer 2/3 (Ctx L2/3), layer 5 (Ctx L5), layer 6 (Ctx L6), and other cortical regions] and subcortical structures [white matter tracts (WMT), caudoputamen (CP), lateral septal complex (LSX), pallidum (PAL), hypothalamus (HY), and the striatum ventral region (STRv)]. Because of the probable dispersion of RNA among nearby spots on the slide during the tissue permeabilization stage, four clusters were composed of spots that could be detected across multiple regions in the tissue which were classified as "unknown" and were excluded from further analysis. As expected, the total number of RNA capture spots and the spatial distribution of each cluster/region was comparable between samples, and thus differential gene expression analysis was performed (Fig. 2D).

As we were able to run spatial transcriptomics on an entire coronal hemisphere, we first quantified differences in gene expression between cortical and subcortical regions (*P*.adj ≤ 0.05 and absolute $\log_2$FC > 0.25) following iTBS and cTBS (data S1 to S4). In agreement with our bulk RNA-seq data, cTBS had a greater influence on the number of DEGs across all brain regions [number of DEGs ranging from 233 (STRv) to 477 (HY)] in comparison to iTBS [number of DEGs ranging from 11 (Ctx L2/3) to 52 (PAL)], 3 hours after stimulation (Fig. 2E). cTBS mostly down-regulated the expression of genes that were seen not only throughout all cortical layers but also across all subcortical structures (Fig. 2F). This predominant

Table 1. Bulk RNA-seq identified several genes that displayed a significant differential expression in the mouse sensorimotor cortex 3 hours following a single session of cTBS. Significant genes were selected based on a $\log_2$FC of > 1 and an adjusted *P* value (*P*.adj) of ≤ 0.05.

Symbol	Gene name	FC	*P*.adj	Function
Crabp1	Cellular retinoic acid binding protein I	1.84	0.04	Signal transduction
Rsf1os1	Remodeling and spacing factor 1, opposite strand 1	−1.77	0.04	DNA repair
Atp6v1b1	ATPase, H+ transporting, lysosomal V1 subunit B1	−1.64	0.05	ATP synthase
Cacna1f	Calcium channel, voltage-dependent, alpha 1F subunit	−1.63	0.02	Voltage-gated ion channel
Teddm1b	Transmembrane epididymal protein 1B	−1.44	0.05	–
Xirp2	Xin actin-binding repeat containing 2	−1.44	0.04	–
Vmn2r84	Vomeronasal 2, receptor 84	−1.35	0.04	Signal transduction
Vmn2r86	Vomeronasal 2, receptor 86	−1.33	0.04	Signal transduction
Muc15	Mucin 15	−1.32	0.04	–
Adam4	A disintegrin and metallopeptidase domain 4	−1.23	0.04	–
Ankrd53	Ankyrin repeat domain 53	−1.23	0.04	Cell division
Plin4	Perilipin 4	−1.10	0.04	Cell death

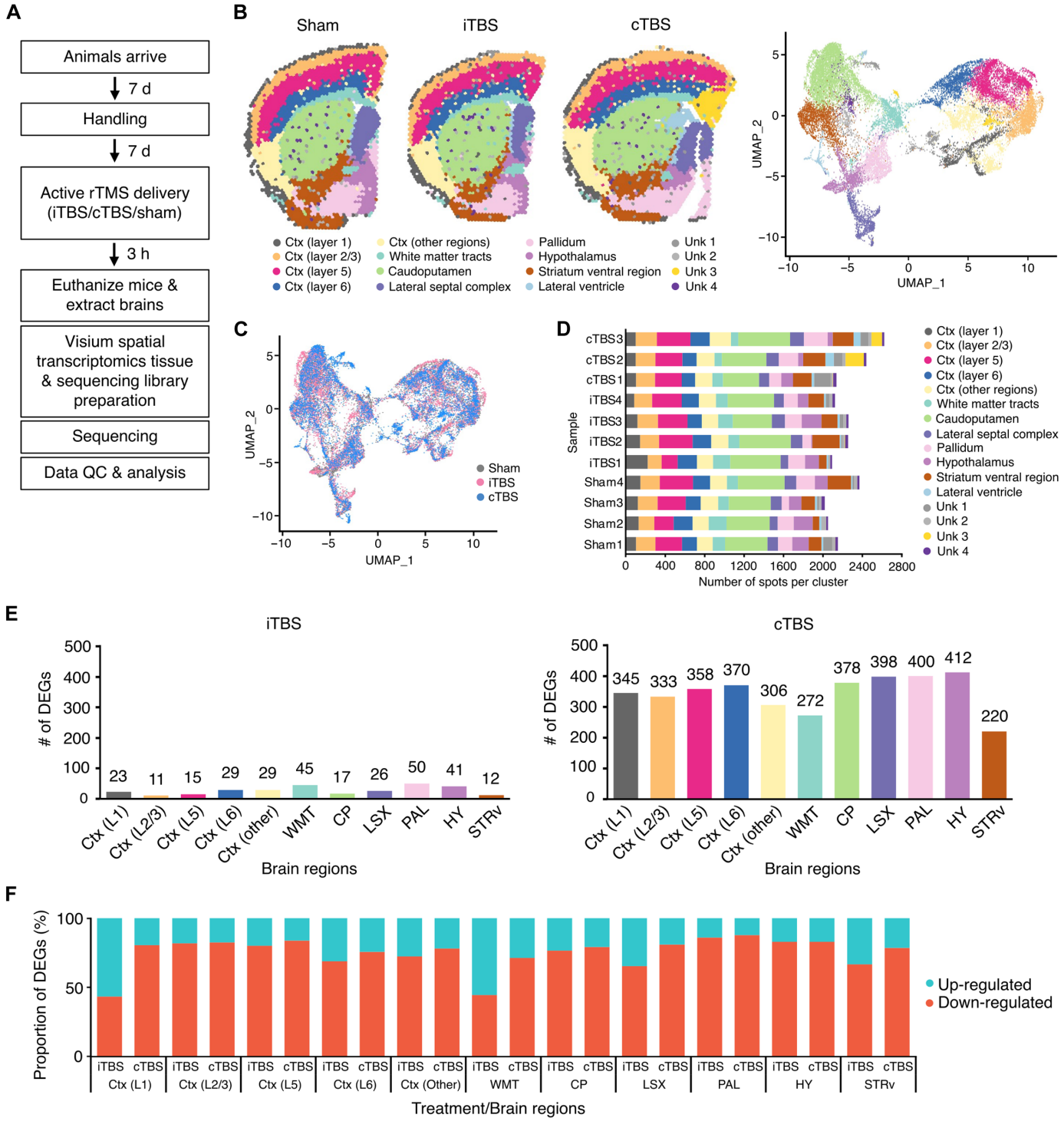

Fig. 2. Brain regions resolved using unsupervised clustering analysis of spatial transcriptomics data from iTBS, cTBS, and sham-stimulated mice. (**A**) Overview of the spatial transcriptomics workflow performed on mice that received iTBS ($n = 4$), cTBS ($n = 3$), or sham stimulation ($n = 4$). (**B**) Representative plots of spatial transcriptomics data from each treatment group, colored based on the clusters identified by unsupervised clustering analysis. Clusters were manually annotated based on their anatomical location using the Allen Mouse Brain Atlas as a reference. Distinct transcriptome profiles can be seen between cortical and subcortical clusters, as visualized on a Uniform Manifold Approximation and Projection (UMAP) plot. (**C**) UMAP plots of treatment groups following correction for any batch effects between samples. (**D**) Number of spots corresponding to each cluster display little variation between samples. (**E**) Number of genes that had a significant change in expression ($P.\text{adj} \leq 0.05$, $\log_2\text{FC} > 0.25$) in each annotated cluster, 3 hours following iTBS and cTBS, and (**F**) the proportion of those genes that were up-regulated and down-regulated. Full list of DEGs can be found in data S3 and S4. Reported *P*.adj values are *P* values that have been adjusted for multiple comparisons for genes in each brain region/cortical layer, using the Bonferroni correction method.

down-regulation of gene expression was also seen in both cortical and subcortical regions following iTBS, with the exception of cortical layer 1 and white matter tracts that had a marginally higher proportion of up-regulated genes. Despite targeting the stimulation to the M1 and SS (i.e., having the highest E-field intensity), the transcriptional profiles of subcortical structures showed a larger difference in the number of DEGs compared to cortical regions following both iTBS and cTBS. This was reflected by the greatest number of differential gene expression changes occurring in the pallidum, white matter tracts, and hypothalamus following iTBS and in the hypothalamus, lateral septal complex, and pallidum following cTBS (Fig. 2E). Although there was some overlap in the significant gene changes induced by iTBS and cTBS, each stimulation protocol also had distinct transcriptional effects in each subcortical structure (Fig. 3, A to F). To get a broad insight into the functional implications of the significant DEGs, we manually assigned each gene into one of seven categories, relating to neural processes of interest, based on its known function in the literature (Fig. 3G; see full list of DEGs with their corresponding annotations in data S3). Following both iTBS and cTBS, we identified the largest number of genes involved in various processes occurring at the synapse or having a role in mediating synaptic plasticity. We found no evidence of changes in genes involved in neurogenesis across all subcortical regions following iTBS, with changes to genes related to intrinsic plasticity and neurotrophic factors also found to be limited across subcortical structures. As cTBS had a greater influence on the expression of genes throughout the brain, genes involved in various plasticity processes (e.g., synaptic, intrinsic, and myelin plasticity), as well as other neural functions (e.g., neurotransmitters, neurogenesis, neurotrophins, and inflammation), were found to be affected in all subcortical regions (Fig. 3G).

Using GO enrichment analysis, we further explored the biological significance associated with the genes altered following iTBS and cTBS within each subcortical region (fig. S2 and data S4). To gain an understanding of the directionality by which various processes/functions were being affected, separate GO analysis was performed on up-regulated and down-regulated DEGs. Considering the substantial number of GO terms identified, we manually assigned the GO terms into higher-order neural plasticity mechanism groups to better contextualize the effects of each stimulation on different brain regions (tables S1 and S2). We found a large number of GO terms relating to oligodendrocytes and myelin, such as oligodendrocyte differentiation, gliogenesis, and myelination, which were enriched in the up-regulated DEGs within the white matter tracts following iTBS (table S1 and data S4). Some examples of the genes implicated in these white matter tract–specific responses following iTBS include myelin-associated glycoprotein *Mag*, CNS-specific myelin protein *Opalin*, and glial cell differentiation regulator *Metrn*. In conjunction with the up-regulation of various myelin plasticity mechanisms in the white matter tracts, GO analysis of down-regulated DEGs within the same region identified several terms related to synaptic plasticity, such as G protein–coupled receptor binding and dendritic spines. Within these GO terms, we identified an enrichment of genes associated with dopaminergic signal transduction including the dopamine- and cyclic adenosine monophosphate–regulated phosphoprotein gene *Ppp1r1b*, calbindin *Calb1*, and a gene belonging to the phosphodiesterase family *Pde1b* (table S1 and data S4). Apart from white matter tracts, little to no GO terms relating to the high-order neural plasticity groups were categorized within the other subcortical regions following iTBS. Instead, beyond neural plasticity mechanisms, we observed an enrichment of mitochondrial-associated processes particularly among down-regulated genes in the pallidum. In addition, GO terms relating to ribosomal functions were found to be enriched among up-regulated genes in the hypothalamus, as well as down-regulated genes in the pallidum (data S4). In contrast, following cTBS, we identified changes in multiple neural plasticity mechanisms across all subcortical regions, with a predominant enrichment of synaptic plasticity– and neurotransmitter-related GO terms among down-regulated genes (table S2 and data S4). Alongside these synaptic changes, we also observed the down-regulation of genes that were classified into various intrinsic plasticity mechanisms, such as "ion channel regulatory activity" and "regulation of membrane potential." These include genes encoding subunits on sodium voltage-gated channels *Scn4b*, potassium voltage-gated channels *Kcna2*, and the ankyrin B scaffolding protein *Ank2*. Although our findings indicate that cTBS modulates a wider range of neural plasticity mechanisms, we also identified processes relating to different aspects of cell death, for example, the "cellular response to oxidative stress" and "regulation of apoptotic signaling pathway," which were enriched in both up-regulated and down-regulated gene sets across all subcortical regions.

TBS protocols induce distinct plasticity mechanisms that are specific to the M1 or SS

The use of rodent-specific coils allowed us to focus the peak-induced electric field strength toward the M1 and SS. Therefore, based solely on stimulation intensity, it could be expected that rTMS would induce the same gene expression changes in the M1 and SS. Given the resolution of spatial transcriptomics, we were able to separate the M1 and SS from one another and investigate this directly. To distinguish between the two cortices, we registered each hematoxylin and eosin (H&E)–stained tissue image to the Allen Mouse Brain Atlas, creating an anatomical map specific to each sample. Previously annotated cortex-specific clusters were then selected, and the corresponding atlas maps were overlaid on the subsetted clusters, allowing the manual selection of Visium spots that aligned to the M1 or SS (Fig. 4, A and B). Through comparisons between iTBS and sham-stimulated tissue, we identified 14 DEGs (4 up-regulated and 10 down-regulated) in the M1 and 20 DEGs (2 up-regulated and 18 down-regulated) in the SS (Fig. 4C). Again, cTBS had a larger effect on both the M1 and SS compared to iTBS, with 426 DEGs (67 up-regulated and 359 down-regulated) and 328 DEGs (70 up-regulated and 258 down-regulated) found in each respective cortical region (Fig. 4C). Several genes were found to be differentially expressed across both regions (8 genes shared between the M1 and SS following iTBS and 262 genes with cTBS), indicating a number of genes modulated by iTBS and cTBS that are not cortical region–specific (see full list of DEGs in data S5).

We found changes in notable myelin marker genes (*Mbp* and *Mobp*) that displayed a decrease in expression solely in the M1 following iTBS (Fig. 5A and fig. S3A). Although GO enrichment analysis of genes affected by cTBS also identified the enrichment of genes, in both the M1 and SS, that were grouped as part of the "myelin sheath" gene set, many were not directly related to myelin and were unexpectedly related to various mRNA, DNA, and ribosomal regulatory processes (e.g., *Rps27a*, *Gapdh*, *Eno1*, etc.; see full lists in data S6). Instead, following cTBS, we identified changes in well-characterized markers for excitatory neurons (*Camk2a*) and inhibitory neurons

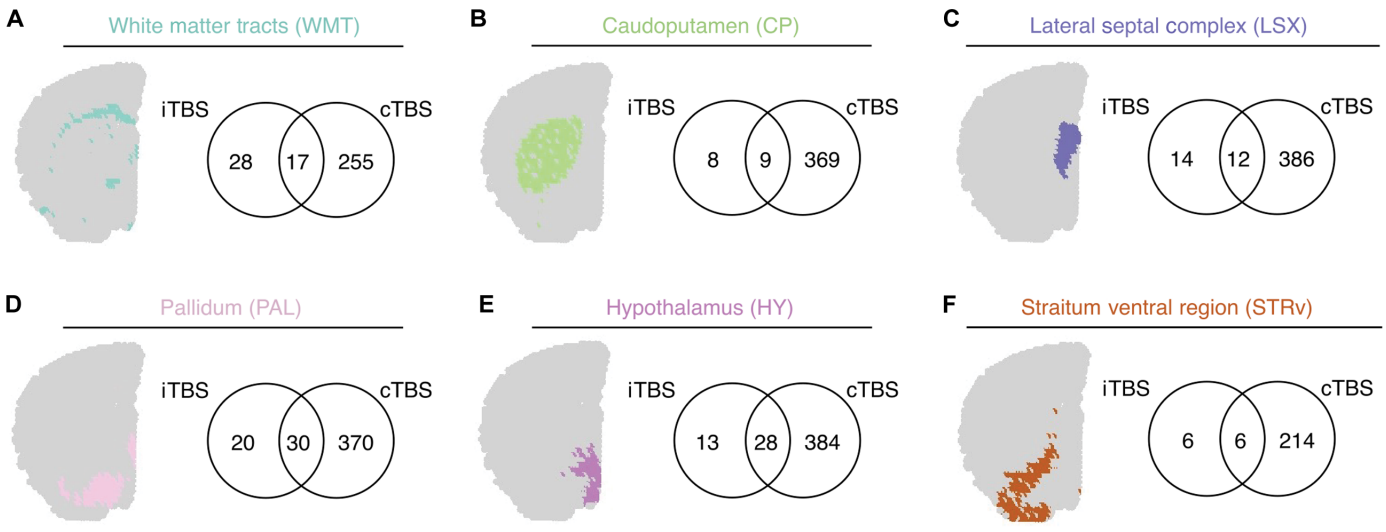

G

	iTBS						cTBS					
	WMT	CP	LSX	PAL	HY	STRv	WMT	CP	LSX	PAL	HY	STRv
Synapse/synaptic plasticity	10	3	8	7	7	3	31	46	52	40	37	32
Neurotransmitter	1	–	2	1	1	–	6	10	10	12	8	8
Intrinsic plasticity/ membrane excitability	2	–	–	–	3	–	7	9	7	12	13	3
Oligodendrocyte/ myelin	4	–	1	–	2	2	10	8	11	9	7	5
Neurogenesis	–	–	–	–	–	–	2	6	6	5	4	4
Neurotrophin	2	–	–	–	–	–	2	5	2	3	1	3
Inflammation/ apoptosis	–	1	1	5	3	2	15	21	18	29	24	16

Fig. 3. Differential gene expression analysis of different subcortical regions 3 hours following iTBS and cTBS in the mouse brain. Spatial plots depicting the anatomical location of clusters that were annotated as various subcortical structures: (**A**) white matter tracts, (**B**) caudoputamen, (**C**) lateral septal complex, (**D**) pallidum, (**E**) hypothalamus, and (**F**) striatum ventral region based on the Allen Mouse Brain Atlas. Venn diagrams display the overlap of significant DEGs (*P*.adj ≤ 0.05, $\log_2$FC > 0.25) identified in each corresponding brain region 3 hours post-iTBS and cTBS. (**G**) Significant DEGs within each subcortical region, where possible, were classified into different neural processes based on their known function. Number of DEGs identified for each neural process, within each brain region following iTBS ($n = 4$) and cTBS ($n = 3$), are shown. Dashes indicate that no DEGs were identified for that functional category. Full list of DEGs can be found in data S4. Reported *P*.adj values are *P* values that have been adjusted for multiple comparisons for genes in each brain region using the Bonferroni correction method.

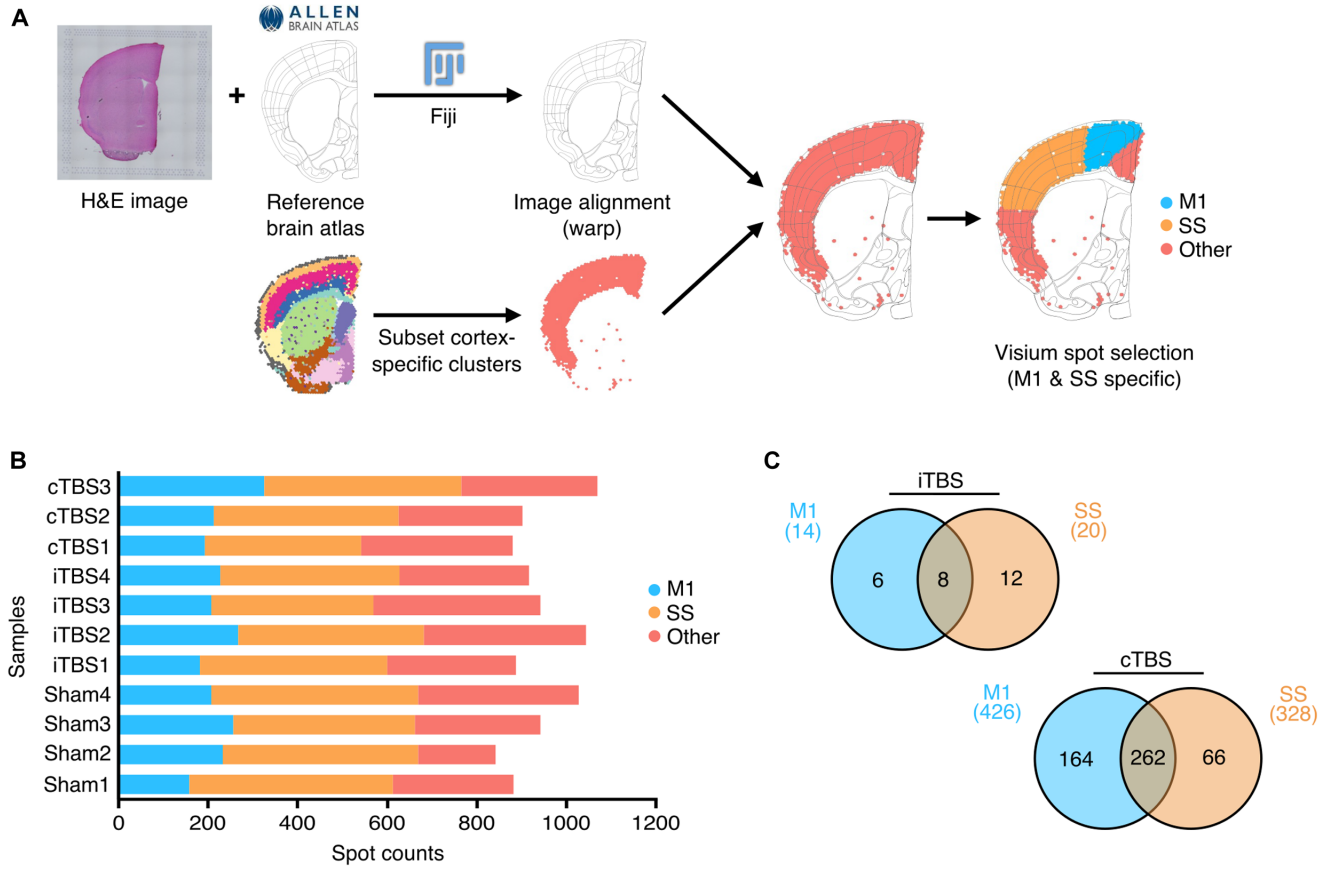

Fig. 4. M1 and SS display different transcriptional responses 3 hours following iTBS and cTBS. (**A**) Outline of the image atlas registration workflow used to manually select Visium spots overlying the M1 and SS. (**B**) Number of spots corresponding to the M1, SS, and other cortical regions across all samples. (**C**) Venn diagram displaying the overlap of genes that had a significant change in expression (*P*.adj ≤ 0.05, $\log_2$FC > 0.25) between iTBS ($n = 4$) and cTBS ($n = 3$) in the M1 cortex (top) and SS (bottom). Full list of DEGs can be found in data S5. Reported *P*.adj values are *P* values that have been adjusted for multiple comparisons for genes in each brain region using the Bonferroni correction method.

(*Pvalb* and *Sst*) that were seen across both the M1 and SS (Fig. 5, B and C). Contrastingly, *Camk2a* was identified to be down-regulated across both cortical regions whereas *Pvalb* displayed an increased in expression within the same regions following cTBS. *Sst*, a gene expressed in another subset of inhibitory interneurons, was found to have a decrease in expression only within the M1 following cTBS. In line with the neuronal gene changes identified, we found several GO terms implicated in aspects of synaptic and intrinsic plasticity across both cortical regions following cTBS, most of which were down-regulated in expression (Fig. 5, D and E; full lists can be found in data S6). In particular, cTBS decreased the expression of numerous genes encoding for proteins involved in neurotransmitter transport and/or release (e.g., *Snap25*, *Snca*, *Stxbp1*, *Syn1*, etc.; Fig. 5D), synaptic function (e.g., *Camk2a*, *Syngap1*, *Nrn1*, *Shank1*, etc.), and synapse structure (e.g., *App*, *Pacsin1*, *Ppp1r9b*, etc.). These synaptic plasticity changes were also accompanied by decreases in GO terms relating to intrinsic plasticity such as "voltage-gated ion channel activity" (e.g., *Scn1a*, *Scn2a*, *Kcn2a*, *Cacna2d1*, etc.; Fig. 5E), "regulation of postsynaptic membrane potential" (e.g., *Slc8a2*, *Gabra3*, *Stx1b*, etc.), and "sodium ion transport" (e.g., *Slc4a10*, *Slc6a1*, *Slc1a2*, *Gria2*, etc.).

Subclustering of the M1 and SS reveals cortical layer–specific effects of TBS protocols

Expanding on our subset analysis of the M1 and SS, we used the power of spatial transcriptomics to further discern whether the effects of rTMS stimulation were occurring within specific layers of the M1 and SS. To explore this, we individually subsetted the M1- and SS-specific spots and again performed unbiased clustering analysis to reveal distinct cortical layers specific to each cortical region (Figs. 6A and 7A).

In the M1, subclustering analysis identified four clusters that anatomically corresponded to the various cortical layers (as defined by the Allen Mouse Brain Reference Atlas). These were annotated as cortical layer 1, cortical layer 2/3, cortical layer 5, and cortical layer 6 (Fig. 6, A and B). Because of the variable number of cortical layer 1 spots between samples, with some having only four or five spots, further differential expression analysis was not performed on this cortical layer (Fig. 6C). As seen previously, both TBS protocols predominantly induced a down-regulation of gene expression across all cortical layers (Fig. 6D). Of the M1 layers, iTBS had the greatest influence on cortical layer 5, whereas cTBS instead had the greatest influence on cortical layer 2/3 (Fig. 6E). Similar to our analysis of

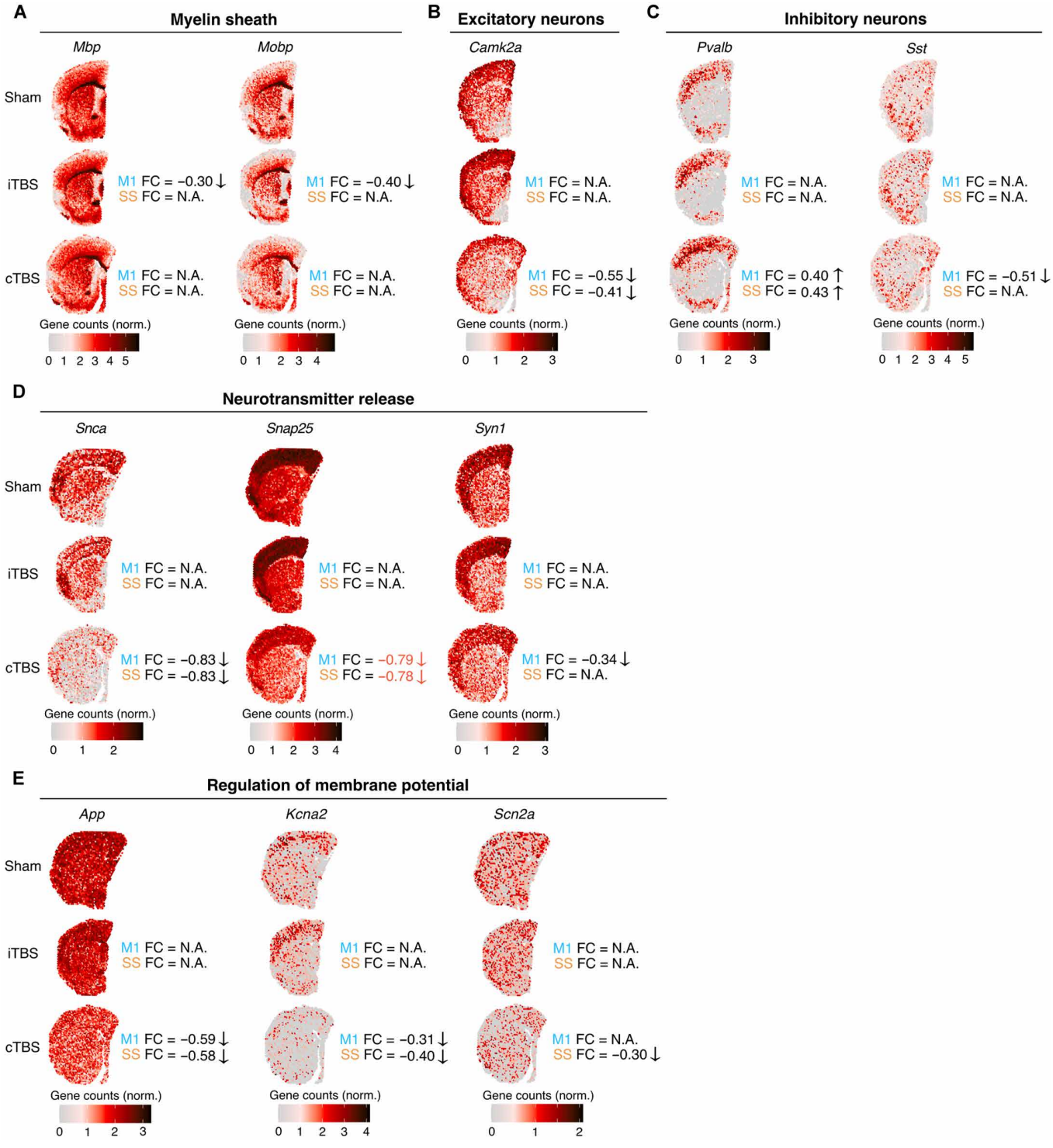

Fig. 5. Spatial expression signatures of representative genes relating to various neural structures/processes. Normalized counts were plotted across representative spatial sections from sham-treated ($n = 4$), iTBS-treated ($n = 4$), and cTBS-treated ($n = 3$) groups for DEGs associated with (**A**) myelin, (**B**) excitatory neurons, (**C**) inhibitory neurons, (**D**) neurotransmitter release, and the (**E**) regulation of membrane potential. All genes were identified to have significant change in expression ($P.\text{adj} \leq 0.05$, $\log_2\text{FC} > 0.25$) in either the M1 or SS 3 hours following iTBS or cTBS. The corresponding $\log_2\text{FC}$ of genes within specific cortical regions are displayed. Volcano plots containing the normalized counts for each gene across all samples can be found in fig. S4. Reported *P*.adj values are *P* values that have been adjusted for multiple comparisons for genes in each brain region using the Bonferroni correction method. N.A., not applicable.

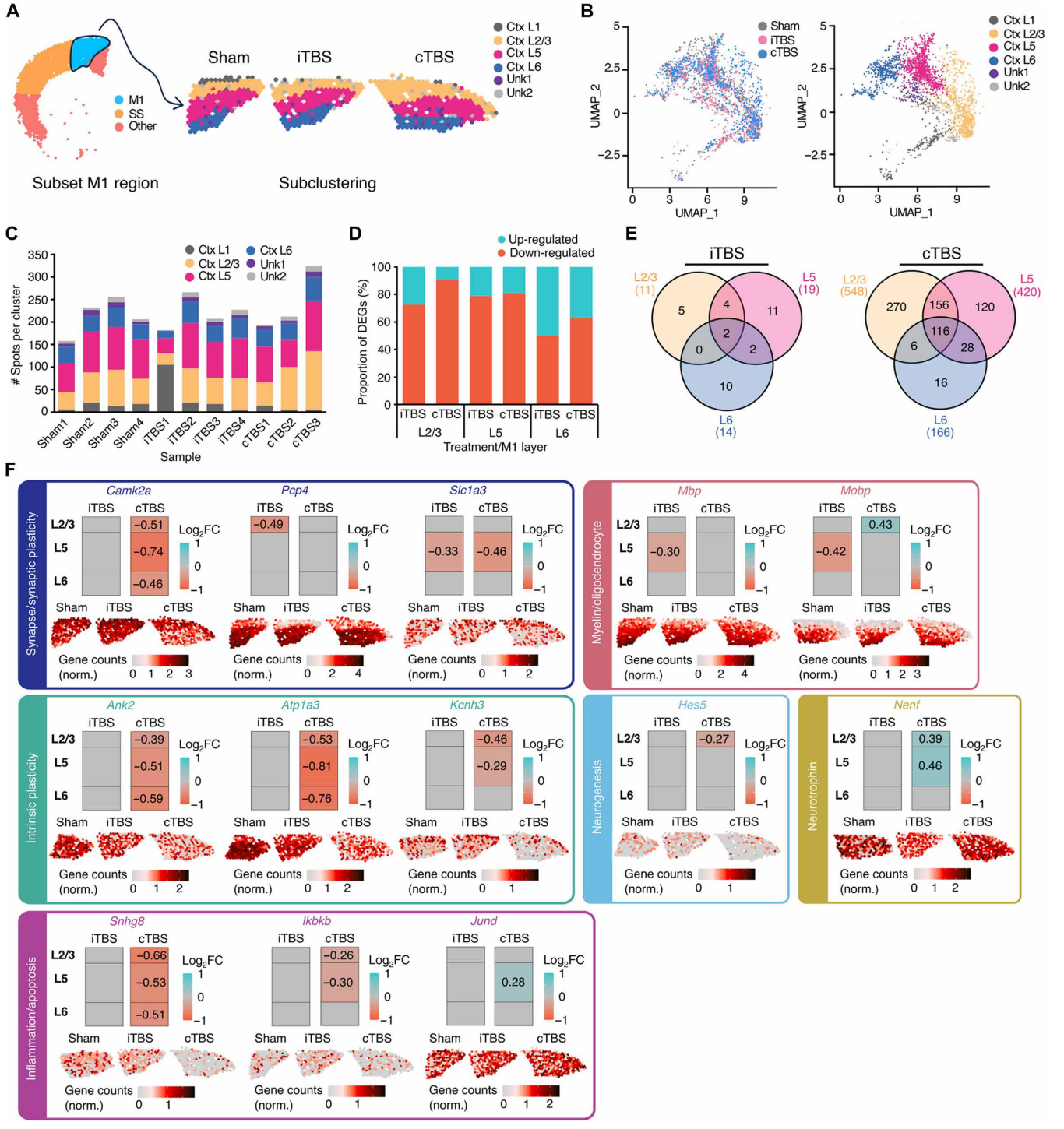

Fig. 6. Subclustering analysis of the M1 spots. (**A**) Visium spots corresponding to the M1 cortex were subsetted and reclustered to resolve four distinct cortical layers. (**B**) UMAP plots colored by treatment group (left) and subclusters (right) of M1 cortex spots. (**C**) Bar plot displaying the number of spots per cluster between all samples. As the number of spots annotated as "cortical layer 1 (Ctx L1)" was sparse in most of the samples, these were not included in the downstream differential expression analyses. (**D**) Bar plot of the proportion of up-regulated and down-regulated DEGs in each M1 cortical layer, following iTBS and cTBS. (**E**) Venn diagram showing the overlap of significant DEGs between M1 cortical layers 2/3, 5, and 6, 3 hours following iTBS (left, $n = 4$) and cTBS (right, $n = 3$). (**F**) Examples of genes that display a significant differential expression, in one or more M1 cortical layers, following either iTBS and/or cTBS stimulation. Genes displayed were identified to be involved in one of six different neural processes based on their known function. For each gene, columns display the $\log_2$FC of the corresponding gene for each of the M1 cortical layers 2/3, 5, and 6 following iTBS and cTBS. Below, normalized counts for each gene were plotted across the best representative M1 cortex spatial section from a sham, iTBS, and cTBS treatment group. Complete lists of DEGs and GOs affected by iTBS and cTBS for each M1 cortex layer can be found in data S7 and S8. For analysis, DEGs were considered significant based on a threshold of *P*.adj ≤ 0.05 and $\log_2$FC > 0.25. Reported *P*.adj values are *P* values that have been adjusted for multiple comparisons for genes in each brain region/cortical layer, using the Bonferroni correction method.

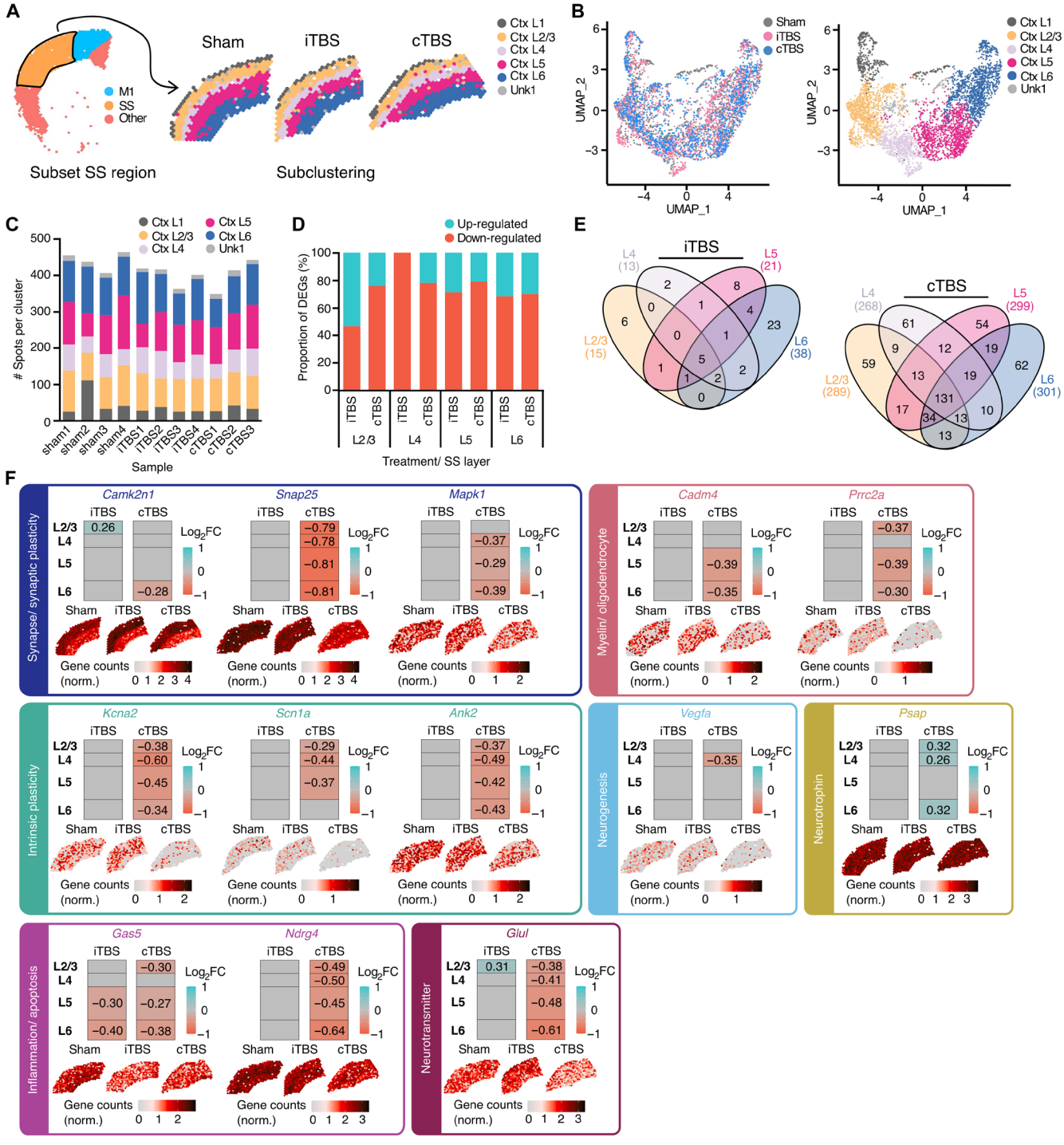

Fig. 7. Subclustering of SS spots. (**A**) Visium spots corresponding to the SS were subsetted and reclustered to resolve five distinct cortical layers. (**B**) UMAP plots colored by treatment group (left) and subclusters (right) of SS spots. (**C**) Bar plot displaying the number of spots per cluster between all samples. Spots corresponding to cortical layer 1 (Ctx L1) were not included in the downstream differential expression analysis due to their sparse distribution across samples. (**D**) Bar plot of the proportion of up-regulated and down-regulated significant, DEGs in each SS cortical layer, 3 hours following iTBS ($n = 4$) and cTBS ($n = 3$). (**E**) Venn diagram showing the overlap of DEGs between SS cortical layers 2/3, 4, 5, and 6, following iTBS (left) and cTBS (right). (**F**) Examples of genes that display a significant differential expression, in one or more M1 cortical layers, following either iTBS and/or cTBS stimulation. Genes displayed were identified to be involved in one of seven different neural processes based on their known function. For each gene, columns display the $\log_2$FC of the corresponding gene for each of the SS cortical layers 2/3, 4, 5, and 6 following iTBS and cTBS. Below, normalized counts for each gene were plotted across the best representative SS spatial section from a sham, iTBS, and cTBS treatment group. Complete lists of DEGs and GOs affected by iTBS and cTBS for each SS layer can be found in data S9 and S10. For analysis, DEGs were considered significant based on a threshold of *P*.adj ≤ 0.05 and $\log_2$FC > 0.25. Reported *P*.adj values are *P* values that have been adjusted for multiple comparisons for genes in each brain region/cortical layer, using the Bonferroni correction method.

subcortical regions, significant DEGs identified in each of the three M1 layers were categorized into higher-order functional categories relating to various neural processes (Table 2 and Fig. 6F; see full list of DEGs in data S7). Broadly, we found evidence of iTBS inducing changes in genes relating to synaptic plasticity (e.g., *Slc1a3* and *Pcp4*; Fig. 6F) and myelin (e.g., *Mbp* and *Mobp*; Fig. 6F), most of which were altered within layer 5 of the M1. As cTBS induced the greatest number of gene expression changes across all cortical layers, we found changes in genes relating to synaptic plasticity (e.g., *Camk2a* and *Slc1a3*; Fig. 6F), myelin (e.g., *Mobp*; Fig. 6F), intrinsic plasticity (e.g., *Ank2*, *Atp1a3*, and *Kcnh3*; Fig. 6F), neurogenesis (e.g., *Hes5*; Fig. 6F), neurotrophins (e.g., *Nenf*; Fig. 6F), and inflammation (e.g., *Snhg8*, *Ikbkb*, and *Jund*; Fig. 6F), all of which displayed varying levels of expression change and regulation. Furthermore, GO analysis identified a considerable number of terms that we manually assigned into high-order neural plasticity groups to better explore the effects of each stimulation on the different M1 layers (tables S3 and S4; see full GO lists in data S8). We found that the aforementioned myelin-related changes identified in the M1 following iTBS appeared only in cortical layer 5 (fig. S5 and table S3). A number of gene sets related to the regulation of apoptosis were enriched among DEGs that were up-regulated following cTBS, particularly relating to a number of intrinsic apoptotic pathways [e.g., the p53 pathway involved in the cellular stress response (*17*)], which were found across all M1 layers. Gene sets broadly relating to neurogenesis and neurotrophin functions were found only in cortical layer 2/3 among down-regulated DEGs following cTBS. Given that cTBS induced the largest number of gene expression changes in cortical layer 2/3, we identified the greatest number of GO terms relating to aspects of the synapse and/or synaptic plasticity and intrinsic plasticity and/or membrane excitability within this region (table S4). However, gene sets relating to neurotransmitters were the least enriched within down-regulated DEGs in M1 layer 2/3, with only 13 GO terms manually assigned to this group, in comparison to 34 terms in cortical layer 5 and 20 terms in cortical layer 6 (table S4).

In the SS, we identified five distinct clusters that were annotated as cortical layer 1, cortical layer 2/3, cortical layer 4, cortical layer 5, and cortical layer 6 (Fig. 7, A and B), using the Allen Mouse Brain Atlas as a reference. Notably, our subclustering analysis of the SS was able to additionally define cortical layer 4, classically found only in the SS but not the M1 (*18*, *19*) (Fig. 7A). Similar to our assessment of the M1 subclusters, we excluded cortical layer 1 in our differential expression analysis due to the low number of spots across all samples (Fig. 7C). We found that both iTBS and cTBS largely induced a down-regulation of genes across all layers within the SS (Fig. 7D). In particular, iTBS had the greatest effect on gene expression within SS layer 6, with a total of 23/39 genes uniquely differentially expressed with that region (Fig. 7E). Similarly, cTBS induced changes in the greatest number of genes within cortical layer 6, although the number of unique DEGs between all cortical layers were comparable (54/236 unique DEGs in cortical layer 5 to 62/236 in cortical layer 6; Fig. 7E). Looking at the known function of DEGs within each SS layer, we found changes in notable synaptic plasticity–related (e.g., *Camk2n1*), neurotransmitter-related (e.g., *Glul*), and inflammatory-related (e.g., *Gas5*) genes following iTBS (Fig. 7F and Table 3). Little to no genes relating to intrinsic plasticity–related processes were identified across the SS following iTBS. Similarly to the M1, cTBS induced changes across all seven of the different neural processes of interest, with the greatest number of genes identified to be involved in synaptic plasticity (e.g., *Camk2n1*, *Snap25*, and *Mapk1*; Fig. 7F). Although changes to myelin-related genes were also identified following cTBS in the SS (e.g., *Cadm4* and *Prrc2a*; Fig. 7F), these were distinct from those seen to display a significant change in expression following iTBS in the M1. Ribosomal-related genes (e.g., *Rpl35*, *Uba52*, *Rps29*, etc.) were predominant among the genes that had a down-regulated expression across all SS layers following iTBS, with GO enrichment analysis identifying terms such as "structural constituent of ribosome" and "cytoplasmic translation" being common between genes (fig. S6). Unexpectedly, despite the low number of up-regulated genes following iTBS, GO analysis found an enrichment of genes relating to "glial cell projection" (*Glul* and *Kcnj10*) within cortical layer 2/3 and "myelin sheath" (*Gapdh*, *Tuba1a*, and *Tubb4a*) in cortical layer 6 (fig. S6 and table S5). Both *Tuba1a* and *Tubb4a* are genes whose protein products each encodes for α-tubulin and β-tubulin, constituents of microtubules that are critical for neuronal structure (*20*, *21*). Following cTBS, we found numerous ribosomal-related GO terms among up-regulated DEGs, contrary to iTBS. In addition, GO terms corresponding to different aspects of the transcription and translation process of RNA, such as "mRNA 5′-UTR binding" and "tRNA binding," were also up-regulated following cTBS across all SS layers (see full GO lists in data S10). Again, adopting our manual assignment of GO terms into higher-order neural

Table 2. Number of significant DEGs, associated with various neural processes, within the mouse M1 3 hours following a single session of iTBS or cTBS. Genes that displayed a significant difference in expression following iTBS, and cTBS in each M1 cortical layer (L2/3, L5, and L6) were categorized into different neural processes based on their known function. Significant genes had a $\log_2$FC of > 0.25 and an adjusted *P* value of ≤ 0.05. Dashes indicate that no DEGs involved in that neural process were identified. Complete lists of DEGs with the functional class labeled can be found in data S7.

	iTBS			cTBS		
	M1 L2/3	M1 L5	M1 L6	M1 L2/3	M1 L5	M1 L6
Synapse/synaptic plasticity	2	4	–	66	54	18
Neurotransmitter	–	–	–	7	8	6
Intrinsic plasticity/membrane excitability	–	–	–	17	8	3
Oligodendrocyte/myelin	–	3	–	7	6	2
Neurogenesis	–	–	1	5	3	–
Neurotrophins	–	–	–	3	3	1
Inflammation/apoptosis	1	1	–	21	15	4

Table 3. Number of significant DEGs, associated with various neural processes, within the mouse SS 3 hours following a single session of iTBS or cTBS. Genes that displayed a significant difference in expression following iTBS and cTBS in each SS cortical layer (L2/3, L4, L5, and L6) were categorized into different neural processes based on their known function. Significant genes had a $\log_2$FC of > 0.25 and an adjusted *P* value of ≤ 0.05. Dashes indicate that no DEGs involved in that neural process were identified. Complete lists of DEGs with the functional class labeled can be found in data S8.

	iTBS				cTBS			
	SS L2/3	SS L4	SS L5	SS L6	SS L2/3	SS L4	SS L5	SS L6
Synapse/synaptic plasticity	3	2	2	5	33	26	37	35
Neurotransmitter	1	–	1	1	6	6	9	9
Intrinsic plasticity/membrane excitability	1	–	–	–	8	10	11	6
Oligodendrocyte/myelin	–	–	1	–	4	4	6	6
Neurogenesis	–	–	–	–	4	3	3	2
Neurotrophins	–	–	–	–	4	4	2	4
Inflammation/apoptosis	–	1	2	2	15	10	12	16

plasticity groups, we found changes in synaptic and intrinsic plasticity mechanisms across all SS layers following cTBS that were predominately enriched in down-regulated DEGs (table S6). The number of gene sets relating to "intrinsic plasticity and/or membrane excitability" was highest in cortical layers 4 and 5. Similar to the M1, we also identified several apoptosis-related gene sets that were associated to up-regulated DEGs in cortical layers 2/3, 4, and 5. GO terms relating to "neurogenesis" were only identified among down-regulated DEGs in cortical layer 2/3.

DISCUSSION

In this study, we used a combination of bulk RNA-seq and spatial transcriptomics to characterize rTMS neuromodulation in mice following targeted stimulation of the M1 and SS. We show that bulk RNA-seq lacks the spatial resolution to fully characterize the transcriptomic changes induced by rTMS, but this could be overcome with the use of spatial transcriptomics. Our data revealed that iTBS and cTBS to the cortex alters gene expression in cortical and subcortical brain regions and that rTMS alters the expression of genes related to several neural plasticity mechanisms and fundamental cellular processes. A key finding for both stimulation protocols was that the effect of rTMS was not uniform across the brain, and within the cortex, the effect of rTMS varied between the different cortical regions and their respective cortical layers. Generally, cTBS induced a greater change in the number of DEGs compared to iTBS, and although there was some overlap in the DEGs and their associated processes, there were unique transcriptomic changes between the protocols.

From previous studies in rodents, it is known that single-pulse TMS activates neurons in a layer-specific manner (*22*, *23*) and that rTMS induces neuronal and glial plasticity in both superficial and deep cortical layers (*5*, *6*, *24*, *25*), which is not uniform across brain regions. This led us to hypothesize that any transcriptomic changes in the cortex following rTMS would depend on the unique circuit and layer composition of the cortical region investigated. We found that, overall, there was some overlap in the DEGs between the M1 and SS, but most of the changes were dependent on the neural circuit/cortical layer and protocol of TBS. In the M1, iTBS altered the expression of genes related to a range of cellular functions across all layers, oligodendrocyte/myelin plasticity in layers 5 and 6, and synaptic plasticity in layer 6. In contrast, cTBS altered the expression of genes related to a range of cellular functions and synaptic plasticity across cortical layers. In the SS, iTBS altered the expression of a range of cellular functions across all layers and oligodendrocyte/myelin plasticity in layer 6, whereas cTBS altered the expression of genes related to a range of cellular functions, neurotransmitter release, and synaptic plasticity in all layers, as well as intrinsic plasticity in layer 4. These results suggest that iTBS may be more effective at modulating oligodendrocyte/myelin plasticity in the cortex than cTBS, which is supported by previous work in mice that has shown that iTBS but not cTBS up-regulates oligodendrocyte maturation and survival in the M1 (*6*), as well as altered myelin structure following iTBS (*7*). cTBS, on the other hand, appears to have a greater effect on gene expression related to synaptic and intrinsic plasticity (i.e., neuronal plasticity mechanisms) at 3 hours after stimulation. Together, our results show that rTMS acts on neuronal and oligodendrocyte/myelin plasticity mechanisms as well as fundamental cellular functions simultaneously, which to a large degree, is specific to the cortical region, cortical layer, and protocol of rTMS applied.

In clinical and nonclinical populations, neuroimaging studies have shown changes to cortical and subcortical regions outside the targeted stimulation site following TBS (*26*–*29*). Given that the induced electric field decreases exponentially from the coil surface, changes outside the targeted region suggest that rTMS neuromodulation spreads across neural circuits and networks independent of the induced electric field. Our data confirm that this occurs at the transcriptomic level as cortical stimulation led to changes in gene expression in both superficial and deep cortical layers, as well as changes in the underlying white matter tracts and subcortical regions (caudoputamen, hypothalamus, lateral septum, pallidum, and ventral striatum). Unexpectedly, the number of DEGs in these subcortical regions was similar to the number of DEGs in the cortex, further suggesting intensity-independent effects of rTMS. This raises the question of how distant brain regions/circuits undergo neuromodulation. We speculate that rTMS increases neural excitability within the targeted site of stimulation (*24*, *25*), which drives activity-dependent plasticity in downstream circuits through synaptic connectivity (i.e., direct anatomical connections). In our data, this is supported by the fact that all the white matter tracts and subcortical structures we investigated

are known to receive direct monosynaptic input from the M1 and SS (*30*). For example, the striatum is known to receive inputs from the motor cortex via intratelencephalic and pyramidal tract neurons (*31*) and rTMS modulation of these neurons in the cortex may provide a direct pathway to drive plasticity subcortically. The specific transcriptomic changes induced in the white matter tracts and subcortical regions were also brain region/circuit– and protocol-specific. Moreover, the main effect of iTBS was mostly confined to oligodendrocyte/myelin plasticity– and synaptic plasticity–related genes in the white matter tracts with no glial-related changes occurring in the caudoputamen or ventral striatum, and changes related to neurotransmitter release only occurring in the lateral septal complex. In contrast, cTBS had less of an effect on oligodendrocyte/myelin plasticity–related genes but altered the expression of genes related to synaptic plasticity, neurotransmitter release, and intrinsic plasticity in the white matter tracts and all the subcortical regions. Therefore, although newer forms of rTMS, such as temporal interference rTMS (*32*), may provide a more efficient way of inducing plasticity in subcortical regions, our data provide direct evidence that rTMS targeted to the cortex leads to strong modulation of subcortical circuits and recruits neuronal and glial plasticity in these synaptically connected subcortical regions with some degree of protocol specificity.

In addition to identifying the neuronal and glial plasticity mechanisms activated by rTMS, an important finding from our whole transcriptome sequencing was further evidence that rTMS alters the expression of genes related to a wide range of cellular functions (*10*, *14*, *33*). Specifically, we found that cTBS and iTBS altered the expression of genes related to essential cellular functions including mitochondrial function, transcription, translation, and cell death. cTBS in particular led to an up-regulation and down-regulation in the expression of genes related to cell death, apoptosis, and oxidative stress. We suspect that this stress response is nonspecific as cTBS is not known to decrease cell counts relative to sham in the motor or sensory cortices (*6*) and we found no changes to other processes commonly seen with cell death (e.g., inflammation). For the changes to other cellular functions such as mitochondrial function, transcription, and translation, we speculate that these occur in response and/or are required to support the neuronal and glial plasticity mechanisms induced [e.g., a change to fundamental transcription and translation genes is needed to support the synthesis of proteins required for synaptic plasticity (*5*)].

Despite major methodological differences between our study and previous rodent studies that have investigated the mechanisms of TBS rTMS in the motor and sensory cortices (e.g., species, stimulation intensity, number of TBS sessions, anesthesia, etc.), a general comparison reveals common plasticity mechanisms affected by TBS. In particular, our results support previous reports that TBS alters synaptic activity with changes to neurotransmitter synthesis and release (*34*–*36*) as well as synaptic plasticity processes (*25*, *37*). Outside of the synapse, we provide further evidence that TBS can alter neuronal excitability through intrinsic plasticity (*24*, *25*, *38*), and to our knowledge, cTBS-induced intrinsic plasticity has not previously been shown. Another common finding was the action of cTBS on specific inhibitory neuron subtypes. Previous studies have suggested that cTBS affects the dendritic integration of pyramidal neurons by altering the activity of calbindin expressing neurons (*36*, *39*, *40*), a subgroup of somatostatin inhibitory neurons (*9*, *41*) that inhibit pyramidal neuron dendrites (*42*). Our data support this theory as we found decreased expression of the somatostatin gene following cTBS in cortical layers 5 and 6. Furthermore, cTBS altered the expression of the parvalbumin gene in cortical layer 5 that defines another subtype of inhibitory neurons that regulate pyramidal neuron output through perisomatic inhibition. Although cTBS has been shown to affect parvalbumin (*40*, *43*, *44*) and somatostatin neurons before, our results suggest that the effect of cTBS on these inhibitory neurons is more pronounced in deeper cortical layers.

Irrespective of the variability in TBS outcomes (*45*–*47*), iTBS is commonly believed to have a greater effect on neural plasticity measures compared to cTBS. In rodents, this is reflected by a greater change to protein markers of neural activity (*43*, *44*), and in humans, a greater and longer-lasting change to motor-evoked potential amplitudes (*48*). In our outcome measure of DEGs, we found that cTBS often led to a greater number of DEGs and more neural plasticity mechanisms compared to iTBS. From these results, we conclude that at 3 hours post-stimulation, cTBS has a greater and more diverse action on gene expression within the brain relative to iTBS. We stop short of saying cTBS has a greater effect on neural plasticity in general as the number of DEGs is likely to change with time after stimulation. For example, in long-term potentiation (i.e., synaptic plasticity) induced with electrical stimulation, gene expression is altered but the number of DEGs does not peak until 24 hours after stimulation, and the number of DEGs is not proportional to the amount of synaptic potentiation (*49*). Therefore, although our results show which neural plasticity mechanisms iTBS and cTBS are acting on, we caution against the use of the total number of DEGs at one time point to generalize which protocol of TBS has the greatest effect on neural plasticity.

When interpreting our results, it should be noted that we delivered bilateral stimulation and one concern is that inducing neural plasticity in both hemispheres could lead to unpredictable effects due to interhemispheric connectivity. This is certainly a possibility; however, it has been shown in rats that inducing neural plasticity in both SSs with iTBS and cTBS leads to an expected up-regulation and down-regulation of neuronal activity, respectively (*50*), arguing against the idea of unpredictable effects following bilateral stimulation. The other important consideration is that, despite an established use of bilateral stimulation to study the mechanisms of rTMS in rodents (*6*, *7*, *25*, *34*, *35*, *39*, *50*–*52*) or as a treatment in humans (*53*), it may induce different neural plasticity mechanisms compared to unilateral stimulation. Given that our transcriptomic datasets are in agreement with the cellular changes observed in our previous studies that have used bilateral (*6*, *7*) and unilateral stimulation (*5*, *54*) in the mouse motor cortex, our combined work suggests that there is at least some overlap in the mechanisms of unilateral and bilateral rTMS. This is further supported by data from patients with major depressive disorders where bilateral rTMS has the same antidepressant efficacy as unilateral rTMS (*53*, *55*, *56*).

For our study, we were able to mimic human rTMS and target the maximum induced electric field to a small region of the cortex, avoiding direct stimulation of the entire cortex, white matter tracts, and subcortex (*5*). However, improved stimulation focality can only be achieved with lower stimulation intensities (*8*), which, in our experiments, is believed to induce an electric field below the threshold needed to generate an action potential (>150 V/m) (*57*) but well above intensities previously shown to alter motor-evoked potentials (*58*), motor learning (*54*), oligodendrocyte/myelin plasticity (*6*, *7*), intrinsic plasticity (*24*), and synaptic plasticity (*5*, *54*) in rodents. Nevertheless, although we have shown protocol-, brain region–, and cortical layer–specific transcriptomic changes with subthreshold rTMS that is more reflective of "medium intensity rTMS," it is possible that

higher intensities of rTMS with low stimulation focality that do induce action potentials ("high intensity rTMS") would lead to different transcriptomic changes. It is also important to note that our data provide a snapshot of the transcriptomic changes that occur 3 hours poststimulation, and it is highly likely that the transcriptomic and plasticity mechanisms induced by rTMS vary with time after stimulation. For example, intrinsic plasticity is observed immediately after stimulation with iTBS in cortical brain slices (*24*), whereas functional synaptic plasticity is only observed 2 to 4 hours after stimulation in organotypic entorhinohippocampal slice cultures (*1*, *2*). In vivo, iTBS-induced structural synaptic plasticity persists to at least 45 hours after stimulation in cortical pyramidal neurons (*5*) and has previously been suggested to lead to early and late changes to neural activity (*36*). Therefore, although we have provided a critical step to guiding the use of basic and clinical rTMS, it will now be important that future studies map rTMS neuromodulation using different rTMS parameters (e.g., the Food and Drug Administration–approved 10-Hz protocol), brains of different ages and sex, and at several time points after stimulation. Furthermore, as whole transcriptome spatial platforms become cheaper and continue to improve, future studies using larger capture areas with single-cell resolution are needed to determine how far rTMS neuromodulation extends and if the brain region/layer–specific changes of rTMS are shaped by certain cell subtypes.

In conclusion, we have provided high-resolution maps of the cellular mechanisms induced by rTMS across the brain. Our findings show that the effect of rTMS is far-reaching and acts on more molecular mechanisms than previously thought. We show that rTMS neuromodulation, to some extent, is specific to the protocol of rTMS used, brain region, and cortical layer. The knowledge gained should assist in an improved interpretation and use of rTMS to manipulate neural circuits in clinical and nonclinical populations.

MATERIALS AND METHODS

Experimental design

This laboratory study investigated the transcriptomic changes that occur after two commonly used protocols of rTMS relative to control/sham stimulation. Bulk RNA-seq was used to investigate whether gross transcriptomic changes could be detected in the sensorimotor cortex and spatial transcriptomics was used to map transcriptomic changes at a much greater resolution and across an entire hemisphere. We hypothesized that the effect of rTMS across the brain would vary given the unique cellular and circuit composition of different brain regions. Similarly, given that previous studies have shown different effects of rTMS depending on the protocol used, we hypothesized that the iTBS protocol would induce different transcriptomic changes to cTBS.

Young adult mice were randomly allocated to receive a single session of sham, iTBS, or cTBS prior to processing for bulk RNA-seq or spatial transcriptomics at 3 hours after stimulation. Sham stimulation and rTMS were delivered using a rodent-specific rTMS coil that replicates the stimulation focality used in human rTMS and has been shown to induce behavioral and cellular neural plasticity in rodents. Bulk RNA-seq used dissected cortical tissue comprising the M1 and SS (i.e., M1 + SS). Spatial transcriptomics used coronal sections containing the M1 and SS, and the analysis on different brain regions was done through clustering and in reference to the Allen Mouse Brain Atlas.

Animals

Young ($n = 27$; 12 weeks old) male C57BL/6J mice, supplied by the Animal Resource Center (Murdoch, Australia), were used for all experiments. Mice were pair-housed upon arrival and given 7 days of habituation to the facility under a standard 12-hour light/dark cycle with ad libitum access to food and water. All animal procedures were performed in accordance with the National Health and Medical Research Council Australia Code of Practice for the Care and Use of Animals for Scientific purposes following approval by the University of Western Australia animal ethics committee (RA/3/100/1677).

Stimulation parameters and rTMS delivery

Custom-built rodent-specific circular coils (8 mm in height by 8 mm in diameter) (*58*) were used to deliver focal stimulation to freely moving mice. Stimulation was delivered as monophasic pulses (300-μs rise time and 100-μs fall time) produced by a waveform generator (Agilent 33500B, USA) connected to a bipolar operational power supply (KEPCO BOP 100-4 M, USA). These coils replicate the stimulation focality used in clinical rTMS and have been shown to induce similar behavioral and functional changes in rodents [e.g., improved motor learning (*54*) and altered motor-evoked potentials (*58*)]. To reduce the animal's stress during stimulation and ensure a consistent position of the coil on the scalp, all mice were handled for a minimum of 5 min/day for seven consecutive days prior to active rTMS or sham stimulation delivery. During handling, mice were accommodated to the placement of the coil on the surface of the head such that the strongest region of stimulation (i.e., beneath the coil windings) overlaid both hemispheres of the M1 and SS. The TMS power supply (disconnected from the coil) was turned on 3 days into the handling period to acclimatize mice to the noise produced by the stimulator.

Following the handling period, all mice were given a single session of active rTMS or sham stimulation. In both the bulk RNA-seq and spatial transcriptomics experiments, the coil was placed on the scalp to focus the maximum electric field strength onto the M1 and SS cortex. Active rTMS was delivered in the form of TBS (*59*), comprised a pattern of three pulses delivered at 50 Hz repeated in 5-Hz intervals. Two patterns of TBS were tested, intermittent TBS (iTBS: 2-s train of TBS repeated once every 10 s for a total of 192 s, 600 pulses) and continuous TBS (cTBS: 40-s train of TBS, 600 pulses). An input voltage of 60.2 V peak to peak was used to produce a peak electromagnetic field intensity of 210 mT at the base of the coil, as measured using a gauss meter (Hirst GM08). Input voltage to the coil was selected to produce the maximum magnetic field intensity while maintaining the coil temperature at < 37°C throughout the duration of stimulation. On the basis of previous electric field modeling of the rodent-specific coil used, we estimate a peak-induced electric field of ~30 V/m at the cortical surface (*5*), which is similar to the intensities shown to induce synaptic and microglial plasticity in vitro (~19 V/m) (*1*–*4*). At this intensity, we believe that the stimulation reflects "medium intensity rTMS" and is subthreshold relative to motor-evoked potentials as we did not observe any rTMS-induced movements or change in motor behavior during stimulation. Sham stimulation was performed for 192 s under all the same conditions, with the coil unplugged from the stimulation instrument. All mice were euthanized using an overdose of sodium pentobarbital and immediately perfused with 20 ml of ice-cold saline (0.9%) 3 hours following rTMS stimulation, a time frame at which neural plasticity changes have been observed (*1*–*3*, *10*).

Bulk RNA-seq sample preparation and whole transcriptome sequencing

For bulk RNA-seq, right sensorimotor cortices were dissected from iTBS ($n = 5$), cTBS ($n = 5$), and sham-stimulated ($n = 5$) young mice. RNA was extracted using the RNeasy Mini Kit (Qiagen) and RNase-Free DNase Set (Qiagen), following the standard manufacturer's instructions. RNA samples were quantified using a LabChip GX Touch Nucleic Acid Analyzer, and all were verified to have an RNA integrity number (RIN) of > 7 required for sequencing.

All RNA samples were submitted to the Australian Genome Research Facility (AGRF; Melbourne, Australia) for library preparation and RNA-seq. In brief, ribosomal RNAs were depleted from samples using the Illumina Ribo-Zero Plus rRNA Depletion Kit prior to the generation of cDNA libraries. Libraries were prepared using the TruSeq Stranded mRNA Total Library Prep Kit (Illumina) and pooled prior to sequencing. Whole transcriptome RNA-seq was performed on the Illumina NovaSeq 6000, generating 50 million, 150–base pair (bp) paired-end reads using the Illumina DRAGEN BCL Convert 07.021.624.3.10.8 pipeline. Libraries for each animal were run in quadruplicate (i.e., samples run over four sequencing lanes).

Bulk RNA-seq data processing

Raw RNA-seq FASTQ files from each sample were quality checked using FastQC (v.0.11.9) (*60*) to check for any variability among sequencing replicates. Replicates were concatenated, and the first 15 bp of reads were trimmed, using fastp (*61*), before being aligned to the ENSEMBL *Mus musculus* GRCm39 reference genome, using STAR aligner (v.2.7.10a) (*62*).

Visium spatial transcriptomics

A separate group of mice from the bulk RNA-seq experiments were used for spatial transcriptomics. Brains from sham-stimulated ($n = 4$), iTBS ($n = 4$), and cTBS ($n = 4$) mice were removed and dissected along the midline. Right hemispheres from each animal were immediately placed in a prepared embedding mold (1 cm by 1 cm) containing a thin layer of an optimal cutting temperature (OCT) embedding medium, and further OCT was added to cover the tissue, ensuring that no air bubbles were present. Embedded tissues were flash frozen in a bath of isopentane and cooled by liquid nitrogen.

Using a cryostat (CryoStar NX70, Thermo Fisher Scientific), tissue blocks were sectioned coronally to 10 μm in thickness. To assess the RNA quality prior to performing the spatial transcriptomics workflow, 10 to 15 sections were collected from each animal and the RNeasy Mini Kit (Qiagen) and RNase-Free DNase Set (Qiagen) were used to extract RNA as per the manufacturer's instructions. All samples had a RIN of > 8, quantified using a LabChip GX Touch Nucleic Acid Analyzer, and were subsequently used for spatial transcriptomics.

During the Visium spatial transcriptomics workflow, an enzymatic permeabilization step is required to allow for the release of RNA from tissue onto the adjacent capture probes on the glass slide. To determine the optimal permeabilization time, the Visium Spatial Tissue Optimisation Reagents Kit (10X Genomics) was used according to the manufacturer's guidelines. As tissue permeabilization times were not expected to vary between mice of the same species and sex, a separate male C57BL/6J mouse (12 weeks old) was used for all optimization steps. Flash-frozen coronal tissue sections (right hemisphere, 10 μm in thickness) were mounted and fixed onto the eight capture areas of the tissue optimization slide. Various tissue permeabilization times were tested: 3, 6, 12, 18, 24, and 30 min. Fluorescent cDNA was synthesized on the side from the RNA released from tissues, and sections were imaged on a Ti2 inverted microscope (Nikon). Twelve minutes was selected as the optimal permeabilization time based on the highest fluorescence intensity detected with the lowest diffusion signal.

Following assessment of the RNA quality and tissue optimization, 10-μm coronal brain sections from each animal, taken from the same approximate location along the coronal plan (~0.26 to 0.74 mm anterior from bregma), were mounted on the Visium Spatial Gene Expression Slide (10X Genomics). The spatial gene expression protocol was performed according to the manufacturer's instructions. In brief, mounted sections were methanol fixed and stained with H&E for morphological analysis and reference for spatial sequencing data. Stained sections were imaged on a Ti2 inverted microscope (Nikon) at a ×10 magnification (numerical aperture = 0.45, 2424-pixel by 2424-pixel resolution). Raw bright-field images were processed in FIJI Image J.

After imaging, Visium Spatial Gene Expression Slides were incubated with a permeabilization enzyme for 12 min, allowing for poly(A) (polyadenylate) mRNA to be directly captured by spatially barcoded probes on the slide. Reverse transcription and second-strand synthesis was performed, generating cDNA strands on the slide that were released and used to construct a sequencing-ready cDNA library.

All 12 dual-indexed, paired-end cDNA libraries were submitted to the AGRF (Melbourne, Australia) for sequencing. Libraries were sequenced on a NovaSeq 6000 instrument (Illumina) using an S1 100-cycle flow cell, at a sequencing depth of ~100 million to 250 million read pairs per sample. Special sequencing read configurations was performed as described by the Visium protocol: read 1, 28 bp; i7 index, 10 bp; i5 index, 10 bp; and read 2, 90 bp.

Spatial transcriptomics data processing

Raw RNA-seq FASTQ files were aligned to the *Mus musculus* mm10 reference genome and matched with the corresponding H&E tissue images using the 10X Genomics SpaceRanger software (v2.0.0). A summarized count table of genes identified within each spot within the spatial fiducial frame array [i.e., unique molecular identifier (UMI) counts] was also generated. Only spots under the tissue were considered for downstream analysis.

Further processing and analysis were performed using R (v4.1.0). Raw counts and images of all samples were compiled through the spatial transcriptomics toolkit, STUtility (v1.1.1) (*63*), and analyzed using a combination of functions in the package and Seurat (v4.0.3) (*64*). During the quality control assessment of our spatial transcriptomics data, one cTBS-treated sample was flagged with having a higher proportion of spots with no transcripts (i.e., UMIs) detected (fig. S1A). Upon further inspection of the distribution of UMIs per spot across the tissue, cTBS-treated sample number 4 had regions that were not successfully permeabilized, as measured by low transcript numbers, and this sample was therefore omitted from further analyses (fig. S1B). As a result, the final sample size for cTBS was $n = 3$ and $n = 4$ for sham and iTBS. As an extra quality control measure, spots expressing more than 30% of mitochondrial genes were also discarded as they typically reflect a large proportion of dead/lysing cells within the capture area (*65*). The remaining reads were subsequently normalized using the SCTransform function in Seurat to account for heterogeneity in sequencing depth between samples. To identify the effect of the different stimulation protocols on various

brain regions and cortical layers, differential gene expression analysis between TBS and sham-stimulated tissue was performed using the FindMarkers function in Seurat.

Allen Mouse Brain Atlas image registration

Identification of cortical region–specific Visium spots was done using the ManualAnnotation function in STUtility, using the H&E images registered to the Allen Mouse Brain Atlas as a reference. To achieve this, annotated outlines of several coronal sections were obtained from the Allen Mouse Brain Reference Atlas (Mouse, P56, Coronal v.2; images 47, 51, 52, and 53). Outlines were chosen based on how closely they matched with each individual H&E image on an anatomical level. Registration of the atlas outline to each H&E section was then performed in FIJI ImageJ (v.2.14.0) using the BigWarp plugin (*66*).

Statistical analysis

Bulk RNA-seq analysis was done in in R (v4.1.0), where reads were quantified, and a raw count table was generated using GenomicAlignments (v.1.26.0) (*67*). Differential gene expression analysis was performed using the standard DESeq2 (v.1.30.1) (*68*) analysis pipeline where iTBS- and cTBS-treated animals were compared against sham controls. In brief, the Wald test was used to generate *P* values that were adjusted for multiple comparisons through the Benjamini-Hochberg false discovery rate correction (*69*). From the list of DEGs relative to sham with *P*-adjusted values of ≤ 0.05 (data S12), genes of interest were determined by further filtering for genes that had an absolute $\log_2$FC of ≥ 1. Data visualization plots were generated with ggplot2 (v.3.3.3) (*70*).

For spatial transcriptomics data, DEGs were identified using the Seurat FindMarkers function. From the list of DEGs relative to sham with *P*-adjusted values of ≤ 0.05 (data S13 and S14), genes of interest were determined by further filtering for genes that had an absolute $\log_2$FC of ≥ 0.25 (*16*). Visium spots corresponding to each brain region/cortical layer were first subsetted prior to performing differentially expression analysis between treatment groups. Thus, reported *P*.adj values are *P* values that have been adjusted for multiple comparisons for genes in each brain region/cortical layer, using the Bonferroni correction method. GO enrichment analysis and visualization was performed using the clusterProfiler (v.4.2.2) (*71*) and the GO database (*72*). Data plots were generated with *ggplot2* (v.3.3.3) or visualization tools in STUtility (e.g., ST.FeaturePlot).

The main analysis scripts for this manuscript can be found at https://github.com/rebecca-ong/rTMS-spatial.

Supplementary Materials

The PDF file includes:

Figs. S1 to S6
Tables S1 to S6
Legends for data S1 to S14

Other Supplementary Material for this manuscript includes the following:

Data S1 to S14

REFERENCES AND NOTES

1. A. Vlachos, F. Müller-Dahlhaus, J. Rosskopp, M. Lenz, U. Ziemann, T. Deller, Repetitive magnetic stimulation induces functional and structural plasticity of excitatory postsynapses in mouse organotypic hippocampal slice cultures. *J. Neurosci.* **32**, 17514–17523 (2012).
2. M. Lenz, S. Platschek, V. Priesemann, D. Becker, L. M. Willems, U. Ziemann, T. Deller, F. Müller-Dahlhaus, P. Jedlicka, A. Vlachos, Repetitive magnetic stimulation induces plasticity of excitatory postsynapses on proximal dendrites of cultured mouse CA1 pyramidal neurons. *Brain Struct. Funct.* **220**, 3323–3337 (2015).
3. M. Lenz, C. Galanis, F. Müller-Dahlhaus, A. Opitz, C. J. Wierenga, G. Szabó, U. Ziemann, T. Deller, K. Funke, A. Vlachos, Repetitive magnetic stimulation induces plasticity of inhibitory synapses. *Nat. Commun.* **7**, 10020 (2016).
4. A. Eichler, D. Kleidonas, Z. Turi, M. Fliegauf, M. Kirsch, D. Pfeifer, T. Masuda, M. Prinz, M. Lenz, A. Vlachos, Microglial cytokines mediate plasticity induced by 10 Hz repetitive magnetic stimulation. *J. Neurosci.* **43**, 3042–3060 (2023).
5. A. D. Tang, W. Bennett, A. D. Bindoff, S. Bolland, J. Collins, R. C. Langley, M. I. Garry, J. J. Summers, M. R. Hinder, J. Rodger, A. J. Canty, Subthreshold repetitive transcranial magnetic stimulation drives structural synaptic plasticity in the young and aged motor cortex. *Brain Stimul.* **14**, 1498–1507 (2021).
6. C. L. Cullen, M. Senesi, A. D. Tang, M. T. Clutterbuck, L. Auderset, M. E. O'Rourke, J. Rodger, K. M. Young, Low-intensity transcranial magnetic stimulation promotes the survival and maturation of newborn oligodendrocytes in the adult mouse brain. *Glia* **67**, 1462–1477 (2019).
7. C. L. Cullen, R. E. Pepper, M. T. Clutterbuck, K. A. Pitman, V. Oorschot, L. Auderset, A. D. Tang, G. Ramm, B. Emery, J. Rodger, R. B. Jolivet, K. M. Young, Periaxonal and nodal plasticities modulate action potential conduction in the adult mouse brain. *Cell Rep.* **34**, 108641 (2021).
8. Z.-D. Deng, S. H. Lisanby, A. V. Peterchev, Electric field depth–focality tradeoff in transcranial magnetic stimulation: Simulation comparison of 50 coil designs. *Brain Stimul.* **6**, 1–13 (2013).
9. P. L. Ståhl, F. Salmén, S. Vickovic, A. Lundmark, J. F. Navarro, J. Magnusson, S. Giacomello, M. Asp, J. O. Westholm, M. Huss, A. Mollbrink, S. Linnarsson, S. Codeluppi, Å. Borg, F. Pontén, P. I. Costea, P. Sahlén, J. Mulder, O. Bergmann, J. Lundeberg, J. Frisén, Visualization and analysis of gene expression in tissue sections by spatial transcriptomics. *Science* **353**, 78–82 (2016).
10. D. Clarke, J. Beros, K. A. Bates, A. R. Harvey, A. D. Tang, J. Rodger, Low intensity repetitive magnetic stimulation reduces expression of genes related to inflammation and calcium signalling in cultured mouse cortical astrocytes. *Brain Stimul.* **14**, 183–191 (2021).
11. S. Grehl, H. M. Viola, P. I. Fuller-Carter, K. W. Carter, S. A. Dunlop, L. C. Hool, R. M. Sherrard, J. Rodger, Cellular and molecular changes to cortical neurons following low intensity repetitive magnetic stimulation at different frequencies. *Brain Stimul.* **8**, 114–123 (2015).
12. T. Dufor, S. Grehl, A. D. Tang, M. Doulazmi, M. Traoré, N. Debray, C. Dubacq, Z.-D. Deng, J. Mariani, A. M. Lohof, R. M. Sherrard, Neural circuit repair by low-intensity magnetic stimulation requires cellular magnetoreceptors and specific stimulation patterns. *Sci. Adv.* **5**, eaav9847 (2019).
13. A. C. Thomson, G. Kenis, S. Tielens, T. A. de Graaf, T. Schuhmann, B. P. F. Rutten, A. T. Sack, Transcranial magnetic stimulation-induced plasticity mechanisms: TMS-related gene expression and morphology changes in a human neuron-like cell model. *Front. Mol. Neurosci.* **13**, 528396 (2020).
14. M. Weiler, K. C. Stieger, K. Shroff, J. P. Klein, W. H. Wood, Y. Zhang, P. Chandrasekaran, E. Lehrmann, S. Camandola, J. M. Long, M. P. Mattson, K. G. Becker, P. R. Rapp, Transcriptional changes in the rat brain induced by repetitive transcranial magnetic stimulation. *Front. Hum. Neurosci.* **17**, 1215291 (2023).
15. J.-C. Hegenbarth, G. Lezzoche, L. J. De Windt, M. Stoll, Perspectives on bulk-tissue RNA sequencing and single-cell RNA sequencing for cardiac transcriptomics. *Front. Mol. Med.* **2**, 839338 (2022).
16. O. Hahn, A. G. Foltz, M. Atkins, B. Kedir, P. Moran-Losada, I. H. Guldner, C. Munson, F. Kern, R. Pálovics, N. Lu, H. Zhang, A. Kaur, J. Hull, J. R. Huguenard, S. Grönke, B. Lehallier, L. Partridge, A. Keller, T. Wyss-Coray, Atlas of the aging mouse brain reveals white matter as vulnerable foci. *Cell* **186**, 4117–4133.e22 (2023).
17. L. Haronikova, V. Olivares-Illana, L. Wang, K. Karakostis, S. Chen, R. Fåhraeus, The *p53* mRNA: An integral part of the cellular stress response. *Nucleic Acids Res.* **47**, 3257–3271 (2019).
18. G. M. G. Shepherd, Intracortical cartography in an agranular area. *Front. Neurosci.* **3**, 337–343 (2009).
19. F. Scala, D. Kobak, S. Shan, Y. Bernaerts, S. Laturnus, C. R. Cadwell, L. Hartmanis, E. Froudarakis, J. R. Castro, Z. H. Tan, S. Papadopoulos, S. S. Patel, R. Sandberg, P. Berens, X. Jiang, A. S. Tolias, Layer 4 of mouse neocortex differs in cell types and circuit organization between sensory areas. *Nat. Commun.* **10**, 4174 (2019).
20. M. A. Tischfield, E. C. Engle, Distinct α- and β-tubulin isotypes are required for the positioning, differentiation and survival of neurons: New support for the "multi-tubulin" hypothesis. *Biosci. Rep.* **30**, 319–330 (2010).
21. P. W. Baas, A. N. Rao, A. J. Matamoros, L. Leo, Stability properties of neuronal microtubules. *Cytoskeleton* **73**, 442–460 (2016).
22. S. C. Murphy, L. M. Palmer, T. Nyffeler, R. M. Müri, M. E. Larkum, Transcranial magnetic stimulation (TMS) inhibits cortical dendrites. *eLife* **5**, e13598 (2016).
23. B. Li, J. P. Virtanen, A. Oeltermann, C. Schwarz, M. A. Giese, U. Ziemann, A. Benali, Lifting the veil on the dynamics of neuronal activities evoked by transcranial magnetic stimulation. *eLife* **6**, e30552 (2017).

24. A. D. Tang, I. Hong, L. J. Boddington, A. R. Garrett, S. Etherington, J. N. J. Reynolds, J. Rodger, Low-intensity repetitive magnetic stimulation lowers action potential threshold and increases spike firing in layer 5 pyramidal neurons in vitro. *Neuroscience* **335**, 64–71 (2016).
25. K. Hoppenrath, W. Härtig, K. Funke, Intermittent theta-burst transcranial magnetic stimulation alters electrical properties of fast-spiking neocortical interneurons in an age-dependent fashion. *Front. Neural Circuits* **10**, 22 (2016).
26. C. Nettekoven, L. J. Volz, M. Kutscha, E.-M. Pool, A. K. Rehme, S. B. Eickhoff, G. R. Fink, C. Grefkes, Dose-dependent effects of theta burst rTMS on cortical excitability and resting-state connectivity of the human motor system. *J. Neurosci.* **34**, 6849–6859 (2014).
27. I. Alkhasli, K. Sakreida, F. M. Mottaghy, F. Binkofski, Modulation of fronto-striatal functional connectivity using transcranial magnetic stimulation. *Front. Hum. Neurosci.* **13**, 190 (2019).
28. A. Zandvakili, H. R. Swearingen, N. S. Philip, Changes in functional connectivity after theta-burst transcranial magnetic stimulation for post-traumatic stress disorder: A machine-learning study. *Eur. Arch. Psychiatry Clin. Neurosci.* **271**, 29–37 (2021).
29. W. Struckmann, R. Bodén, M. Gingnell, D. Fällmar, J. Persson, Modulation of dorsolateral prefrontal cortex functional connectivity after intermittent theta-burst stimulation in depression: Combining findings from fNIRS and fMRI. *Neuroimage Clin.* **34**, 103028 (2022).
30. Allen Institute for Brain Science, Allen Mouse Brain Connectivity Atlas, https://connectivity.brain-map.org/.
31. G. M. G. Shepherd, Corticostriatal connectivity and its role in disease. *Nat. Rev. Neurosci.* **14**, 278–291 (2013).
32. A. Khalifa, S. M. Abrishami, M. Zaeimbashi, A. D. Tang, B. Coughlin, J. Rodger, N. X. Sun, S. S. Cash, Magnetic temporal interference for noninvasive and focal brain stimulation. *J. Neural Eng.* **20**, 016002 (2023).
33. W. Hwang, J. K. Choi, M. S. Bang, W.-Y. Park, B.-M. Oh, Gene expression profile changes in the stimulated rat brain cortex after repetitive transcranial magnetic stimulation. *Brain Neurorehabil.* **15**, e27 (2022).
34. S. Aydin-Abidin, J. Trippe, K. Funke, U. T. Eysel, A. Benali, High- and low-frequency repetitive transcranial magnetic stimulation differentially activates c-Fos and zif268 protein expression in the rat brain. *Exp. Brain Res.* **188**, 249–261 (2008).
35. J. Trippe, A. Mix, S. Aydin-Abidin, K. Funke, A. Benali, Theta burst and conventional low-frequency rTMS differentially affect GABAergic neurotransmission in the rat cortex. *Exp. Brain Res.* **199**, 411–421 (2009).
36. K. Hoppenrath, K. Funke, Time-course of changes in neuronal activity markers following iTBS-TMS of the rat neocortex. *Neurosci. Lett.* **536**, 19–23 (2013).
37. T.-H. Hsieh, Y.-Z. Huang, A. Rotenberg, A. Pascual-Leone, Y.-H. Chiang, J.-Y. Wang, J.-J. J. Chen, Functional dopaminergic neurons in substantia nigra are required for transcranial magnetic stimulation-induced motor plasticity. *Cereb. Cortex* **25**, 1806–1814 (2015).
38. E. S. King, A. D. Tang, Intrinsic plasticity mechanisms of repetitive transcranial magnetic stimulation. *Neuroscientist* **30**, 260–274 (2024).
39. A. Benali, J. Trippe, E. Weiler, A. Mix, E. Petrasch-Parwez, W. Girzalsky, U. T. Eysel, R. Erdmann, K. Funke, Theta-burst transcranial magnetic stimulation alters cortical inhibition. *J. Neurosci.* **31**, 1193–1203 (2011).
40. A. Mix, A. Benali, K. Funke, Strain differences in the effect of rTMS on cortical expression of calcium-binding proteins in rats. *Exp. Brain Res.* **232**, 435–442 (2014).
41. I. Banovac, D. Sedmak, M. Esclapez, Z. Petanjek, The distinct characteristics of somatostatin neurons in the human brain. *Mol. Neurobiol.* **59**, 4953–4965 (2022).
42. M. Murayama, E. Pérez-Garci, T. Nevian, T. Bock, W. Senn, M. E. Larkum, Dendritic encoding of sensory stimuli controlled by deep cortical interneurons. *Nature* **457**, 1137–1141 (2009).
43. L. J. Volz, A. Benali, A. Mix, U. Neubacher, K. Funke, Dose-dependence of changes in cortical protein expression induced with repeated transcranial magnetic theta-burst stimulation in the rat. *Brain Stimul.* **6**, 598–606 (2013).
44. A. Mix, A. Benali, U. T. Eysel, K. Funke, Continuous and intermittent transcranial magnetic theta burst stimulation modify tactile learning performance and cortical protein expression in the rat differently. *Eur. J. Neurosci.* **32**, 1575–1586 (2010).
45. M. R. Hinder, E. L. Goss, H. Fujiyama, A. J. Canty, M. I. Garry, J. Rodger, J. J. Summers, Inter- and intra-individual variability following intermittent theta burst stimulation: Implications for rehabilitation and recovery. *Brain Stimul.* **7**, 365–371 (2014).
46. A. Jannati, G. Block, L. M. Oberman, A. Rotenberg, A. Pascual-Leone, Interindividual variability in response to continuous theta-burst stimulation in healthy adults. *Clin. Neurophysiol.* **128**, 2268–2278 (2017).
47. R. A. Ozdemir, P. Boucher, P. J. Fried, D. Momi, A. Jannati, A. Pascual-Leone, E. Santarnecchi, M. M. Shafi, Reproducibility of cortical response modulation induced by intermittent and continuous theta-burst stimulation of the human motor cortex. *Brain Stimul.* **14**, 949–964 (2021).
48. M. Wischnewski, D. J. L. G. Schutter, Efficacy and time course of theta burst stimulation in healthy humans. *Brain Stimul.* **8**, 685–692 (2015).
49. M. M. Ryan, B. Ryan, M. Kyrke-Smith, B. Logan, W. P. Tate, W. C. Abraham, J. M. Williams, Temporal profiling of gene networks associated with the late phase of long-term potentiation in vivo. *PLOS ONE* **7**, e40538 (2012).
50. A. Thimm, K. Funke, Multiple blocks of intermittent and continuous theta-burst stimulation applied via transcranial magnetic stimulation differently affect sensory responses in rat barrel cortex. *J. Physiol.* **593**, 967–985 (2015).
51. E. Kloosterboer, K. Funke, Repetitive transcranial magnetic stimulation recovers cortical map plasticity induced by sensory deprivation due to deafferentiation. *J. Physiol.* **597**, 4025–4051 (2019).
52. B. Lippmann, G. Barmashenko, K. Funke, Effects of repetitive transcranial magnetic and deep brain stimulation on long-range synchrony of oscillatory activity in a rat model of developmental schizophrenia. *Eur. J. Neurosci.* **53**, 2848–2869 (2021).
53. L. Chen, A.-R. Hudaib, K. E. Hoy, P. B. Fitzgerald, Is rTMS effective for anxiety symptoms in major depressive disorder? An efficacy analysis comparing left-sided high-frequency, right-sided low-frequency, and sequential bilateral rTMS protocols. *Depress. Anxiety* **36**, 723–731 (2019).
54. A. D. Tang, W. Bennett, C. Hadrill, J. Collins, B. Fulopova, K. Wills, A. Bindoff, R. Puri, M. I. Garry, M. R. Hinder, J. J. Summers, J. Rodger, A. J. Canty, Low intensity repetitive transcranial magnetic stimulation modulates skilled motor learning in adult mice. *Sci. Rep.* **8**, 4016 (2018).
55. J.-J. Chen, Z. Liu, D. Zhu, Q. Li, H. Zhang, H. Huang, Y. Wei, J. Mu, D. Yang, P. Xie, Bilateral vs. unilateral repetitive transcranial magnetic stimulation in treating major depression: A meta-analysis of randomized controlled trials. *Psychiatry Res.* **219**, 51–57 (2014).
56. S. Sehatzadeh, Z. J. Daskalakis, B. Yap, H.-A. Tu, S. Palimaka, J. M. Bowen, D. J. O'Reilly, Unilateral and bilateral repetitive transcranial magnetic stimulation for treatment-resistant depression: A meta-analysis of randomized controlled trials over 2 decades. *J. Psychiatry Neurosci.* **44**, 151–163 (2019).
57. A. S. Aberra, B. Wang, W. M. Grill, A. V. Peterchev, Simulation of transcranial magnetic stimulation in head model with morphologically-realistic cortical neurons. *Brain Stimul.* **13**, 175–189 (2020).
58. A. D. Tang, A. S. Lowe, A. R. Garrett, R. Woodward, W. Bennett, A. J. Canty, M. I. Garry, M. R. Hinder, J. J. Summers, R. Gersner, A. Rotenberg, G. Thickbroom, J. Walton, J. Rodger, Construction and evaluation of rodent-specific rTMS coils. *Front. Neural Circuits* **10**, 47 (2016).
59. Y.-Z. Huang, M. J. Edwards, E. Rounis, K. P. Bhatia, J. C. Rothwell, Theta burst stimulation of the human motor cortex. *Neuron* **45**, 201–206 (2005).
60. S. Andrews, FastQC (Babraham Bioinformatics, 2010).
61. S. Chen, Y. Zhou, Y. Chen, J. Gu, fastp: An ultra-fast all-in-one FASTQ preprocessor. *Bioinformatics* **34**, i884–i890 (2018).
62. A. Dobin, C. A. Davis, F. Schlesinger, J. Drenkow, C. Zaleski, S. Jha, P. Batut, M. Chaisson, T. R. Gingeras, STAR: Ultrafast universal RNA-seq aligner. *Bioinformatics* **29**, 15–21 (2013).
63. J. Bergenstråhle, L. Larsson, J. Lundeberg, Seamless integration of image and molecular analysis for spatial transcriptomics workflows. *BMC Genomics* **21**, 482 (2020).
64. Y. Hao, S. Hao, E. Andersen-Nissen, W. M. Mauck III, S. Zheng, A. Butler, M. J. Lee, A. J. Wilk, C. Darby, M. Zager, P. Hoffman, M. Stoeckius, E. Papalexi, E. P. Mimitou, J. Jain, A. Srivastava, T. Stuart, L. M. Fleming, B. Yeung, A. J. Rogers, J. M. McElrath, C. A. Blish, R. Gottardo, P. Smibert, R. Satija, Integrated analysis of multimodal single-cell data. *Cell* **184**, 3573–3587.e29 (2021).
65. S. Márquez-Jurado, J. Díaz-Colunga, R. P. das Neves, A. Martinez-Lorente, F. Almazán, R. Guantes, F. J. Iborra, Mitochondrial levels determine variability in cell death by modulating apoptotic gene expression. *Nat. Commun.* **9**, 389 (2018).
66. T. B. T. Thuma, J. A. Bogovic, K. B. Gunton, H. Jimenez, B. Negreiros, J. S. Pulido, The big warp: Registration of disparate retinal imaging modalities and an example overlay of ultrawide-field photos and en-face OCTA images. *PLOS ONE* **18**, e0284905 (2023).
67. M. Lawrence, W. Huber, H. Pagès, P. Aboyoun, M. Carlson, R. Gentleman, M. T. Morgan, V. J. Carey, Software for computing and annotating genomic ranges. *PLoS Comput. Biol.* **9**, e1003118 (2013).
68. M. I. Love, W. Huber, S. Anders, Moderated estimation of fold change and dispersion for RNA-seq data with DESeq2. *Genome Biol.* **15**, 550 (2014).
69. Y. Benjamini, Y. Hochberg, Controlling the false discovery rate: A practical and powerful approach to multiple testing. *J. R. Stat. Soc. Series B Stat. Methodol.* **57**, 289–300 (1995).
70. H. Wickham, *Ggplot2: Elegant Graphics for Data Analysis* (Springer-Verlag, 2009); https://ggplot2.tidyverse.org.
71. G. Yu, L.-G. Wang, Y. Han, Q.-Y. He, clusterProfiler: An R package for comparing biological themes among gene clusters. *OMICS* **16**, 284–287 (2012).
72. M. Ashburner, C. A. Ball, J. A. Blake, D. Botstein, H. Butler, J. M. Cherry, A. P. Davis, K. Dolinski, S. S. Dwight, J. T. Eppig, M. A. Harris, D. P. Hill, L. Issel-Tarver, A. Kasarskis, S. Lewis, J. C. Matese, J. E. Richardson, M. Ringwald, G. M. Rubin, G. Sherlock, Gene Ontology: Tool for the unification of biology. *Nat. Genet.* **25**, 25–29 (2000).

Acknowledgments: We thank L. Cocchi, K. Iyer, and J. Reynolds for feedback on the manuscript and N. Matigian for bioinformatics services (Queensland Cyber Infrastructure Foundation).

Funding: This work was supported by a 2021 Western Australian Near Miss Award, 2022 Perron Institute for Neurological and Translational Sciences Internal Award, and Sarich Family Research Fellowship to A.D.T. R.C.S.O. was supported by an Australian Rotary Health/ Gail & Bryan PhD Scholarship. **Author contributions:** Conceptualization: R.C.S.O. and A.D.T. Methodology: R.C.S.O. and A.D.T. Investigation: R.C.S.O. and A.D.T. Data curation: R.C.S.O. Validation: R.C.S.O. and A.D.T. Visualization: R.C.S.O. and A.D.T. Formal analysis: R.C.S.O. and A.D.T. Software: R.C.S.O. Resources: A.D.T. Project administration: R.C.S.O. and A.D.T. Supervision: A.D.T. Writing—original draft: R.C.S.O. and A.D.T. Writing—review and editing: R.C.S.O. and A.D.T. Funding acquisition: R.C.S.O. and A.D.T. **Competing interests:** The authors declare that they have no competing interests. **Data and materials availability:** The data for this study have been deposited in the Gene Expression Omnibus (GEO) database (GSE259403 and GSE259405). All data needed to evaluate the conclusions in the paper are present in the paper and/or the Supplementary Materials.

Submitted 17 March 2024
Accepted 2 December 2024
Published 8 January 2025
10.1126/sciadv.ado6705